(NASA-CR-140257) RESEARCH ON THE THERMAL HISTORY OF THE MOON Final Report, Jun. 1971 - Aug. 1973 (Earth Sciences Research, Inc.) 68 p HC $6.50 CSCL 03B

N74-35241

Unclas
G3/30 49636

ABSTRACT

Lunar thermal history modelling demonstrates that a realistic computer simulation can be used to predict many more observables than heat flow and internal composition. These observables include major and minor element concentrations, thickness of the lunar "crust", intensity of volcanic activity as a function of time, etc.

The models which are most consistent with the observations include: a high surface temperature and low interior temperature during the very early lunar history; high near-surface radioactivity and relatively low radioactivity in the interior; a molten zone formed at or near the surface which gradually migrates downward with time.

Lunar magnetic anomaly calculations show that large anomalies measured at some of the landing sites and above some points on the surface cannot be caused by mere basalts but are consistent with valley fillings of Cayley-like material with a remenant magnetization of about 2×10^{-4} emu/gm.

We also speculate that the source of the magnetic field which must have been present in the early stages of lunar evolution could have been caused by a layer of conducting fluid at a depth of several hundred kilometers which acted to decouple the solid core from a solid crust.

TABLE OF CONTENTS

FIGURES

FORWARD

This report was prepared by Earth Sciences Research Inc. and covers work carried out under contract NAS-9-11968 during the period June 1971 through August 1973. The work was administered by the National Aeronautics Space Administration, Lyndon B. Johnson Space Center, under the technical direction of Dr. Paul W. Gast until his untimely death in 1973. Throughout the program close liason was maintained with Dr. Gast, Dr. David W. Strangway, Dr. Jeff Warner and Dr. Wolfe Gose.

This report presents a summary of the findings of the study, much of which has already been incorporated into publications listed in the back. It also includes some unpublished material related to the thermal history of the moon.

Earth Sciences Research, Inc.

I. INTRODUCTION

Prior to the Apollo landings much effort was devoted to predicting the possible thermal state of the lunar interior. The investigations included development of computer programs to simulate the thermal development of the moon and thus provide a guide for the intelligent and systematic exploration of the lunar surface. Following the landings it was possible to eliminate many lunar history models and to concentrate on refinement of those models which were found to be generally in accord with the evidence obtained from the returned samples and other observations. The present authors had participated in one of the prelanding studies involving development of lunar thermal history simulation programs. Objectives of the research reported here were to employ actual lunar sample data in updating and modifying the existing computer programs in order to provide refined models of geological history of the moon and similar small planets and, subsequently to calculate thermal histories for specific parameters of interest in establishing the evolution of such planetary bodies.

The bulk of the effort was directed towards developing a computer program with the ability to handle such factors as: non-uniform initial composition; arbitrary initial temperature gradients; arbitrary initial distribution of radioactivity; effective latent heat of melting; effects of variable degrees of partial melting; effects of redistribution of heat sources; and effects of variable thermal conductivity. In addition, there were several minor modifications required such as modernizing the computer language, resolving some minor discrepancies in the programs and attempting to eliminate some of the known less realistic aspects of the computer model.

Following completion of the program modifications, and as a result of the Apollo discoveries of a substantial lunar magnetic field, the study was extended to include model calculations on various aspects of the lunar magnetic field including anomalies to be expected above circular craters and anomalies in the neighborhood of several Apollo landing sites.

II. STUDIES OF THE THERMAL HISTORY OF THE MOON

Early calculations by Urey, MacDonald and others were based primarily on the assumption of an initially uniform model of either "chondritic" or "terrestrial" composition and assumed a thermal conductivity in which radiative transfer played a large role. As it was recognized that melting of the lunar interior could significantly influence the thermal history, several attempts were made to take this into account. Fricker, et.al. (1967) allowed for upward diffusion of radioactive elements and assumed that once complete melting had taken place, convective transfer would dominate. McConnell, et.al. (1967), on the other hand neglected convective transfer in the conventional sense, but allowed for transfer to the surface of radioactive elements with the melt, thus simulating diffusion.

More recently new information has been obtained which demonstrates that better models are required. In the first place, analysis of lunar samples shows that an initial uniform chemical composition is no longer tenable, and that neither the "chondritic" nor the "terrestrial" models is suitable for an initial starting composition (Gast, 1971). Furthermore, recent experimental and theoretical studies show that radiative conductivity is unlikely to dominate heat transfer from the lunar interior (Aronson, et.al. 1967, 1970; Fukao, et.al. 1968). Accordingly, Wood (1970), Hays (1971) and Toksoz, et.al. (1971) have incorporated more realistic compositions and thermal conductivities into their models and have attempted to allow for the redistribution of radioactivity at the time of melting.

Even with these improvements however there are no published calculations which intimately associate movement of the radioactive elements with movement of a melt, whose migration is controlled by reasonable mechanical and thermal considerations. Such a model should be capable of predicting a wide variety of properties which could be compared with field observations. Some of these observations are discussed in more detail in the following section.

Observational Constraints on Successful Models

With the rapidly increasing knowledge of the geological, geophysical, and geochemical properties of the moon, the constraints imposed on successful models become more and more stringent. The most important are those related to present interior temperatures, present heat flow composition, density and velocity distributions, strength of the interior, and thermal properties such as specific heat, thermal conductivity, and heat of fusion. In addition, the model must predict times, rates, and volumes of extrusives consistent with those inferred from other studies.

One of the most difficult factors to determine is the present interior temperature. From magnetic observations, Sonnett, et.al. (1970) have inferred temperatures as low as 800° K at 500 kilometers and 1200° K at 1000 kilometers below the surface. Such temperatures are most easily explained by very low uranium concentrations in the deep interior, as pointed out by Hays (1971). Tozer (1971) believes that the equilibrium temperature for convection by means of solid state creep would not be much different than that postulated by Sonnett. Since convection requires an increasing temperature as a function of depth, and the geochemical evidence

suggests that the moon was initially much cooler at depth than near the surface. Tozer's convective transport mechanism is only likely to become effective at those times and in those regions where temperature increases faster than the adiabatic gradiant. In the calculations discussed below, the effects of solid convection are neglected, although we do not believe they should be dismissed.

The presence of mascons provides additional evidence for low interior temperatures. Their maintenance would require enough strength down to 150 kilometers (Kaula, 1969) to maintain stresses on the order of 100 bars over periods of more than 10^9 years. This implies temperatures in the range 900-1100° K or less at these depths since the time that the lunar mare basalts were extruded 3.5 billion years ago.

The only estimate of the lunar heat flow available at the time of the calculation (Langseth, 1971) was 3.3 microwatts per square centimeter. When considered in the light of magnetic and gravitational observations this value was unexpectably large, yet it is consistent with intense volcanic activity in the past and there is no reason at the present time to suggest that it is significantly in error. The possibility exists that conditions at the Apollo 15 landing site are anomalous, but this can only be determined after several different sites have been investigated.

Thus we have two apparently conflicting sets of constraints. The high heat flow and intense volcanic activity suggest extensive melting of the interior both now and in the past. The gravitational and magnetic interpretations seem to

require a moon which is currently relatively cool to depths of at least 200, and possibly 500 kilometers. Whether any model can simultaneously explain the conflicting observations remains to be seen.

As our model allows for redistribution of radioactive elements, and provides an estimate of the average composition of the different portions of the moon as a function of time, the observed surface composition can then be compared with that predicted in order to establish the validity of any model. Unfortunately, current estimates of the overall surface composition are based on samples derived almost exclusively from the maria which is representative of less than half of the total lunar surface. However, the composition of the basalts generated in the interior must be consistent with the average basalts seen on the surface. This means that the uranium concentration for the mare basalts generated about 3.5×10^9 years ago must be approximately 0.25 ppm uranium and 500 ppm potassium.

The model should also predict an initial period of melting and extrusion whose age is greater than 4.4×10^9 years and a second period of extrusion centered around 3.5×10^9 years ago, which lasts for approximately 10^9 years. Minor isolated volcanic activity throughout the reaminder of the moon's history is permitted.

The redistribution of major components implies a change in density distribution with depth which also must be reflected in the moment of inertia. This requires a knowledge of specific volume of material as a function of pressure and temperature. At the present time we are assuming that the density of the low

melting phase both in its solid and liquid states is 3.2 grams/cc and the high melting phase is 3.4 grams/cc. Because of this obvious oversimplification of the density of the major phases, no attempt has been made to calculate the moment of inertia.

Geometrical, Compositional and Thermal Parameters

As a first step in developing a more geologically complete model we modified our previous computer programs to bring them to a level of sophistication sufficient to incorporate the following features:

1. A nonuniform initial composition in terms of fraction of low melting to high melting phase present and for variation in the uranium, potassium, and thorium contents as a function of depth.
2. Partitioning of the radioactive elements between the melt and the solid phases.
3. A cutoff value of melt which must be exceeded before magma can move to the surface.

The model is in many ways similar to that described in a previous paper (McConnell, et.al. 1967). As in the previous model, the moon is broken up into a number of zones. For the calculations described below each zone was taken to be 20 kilometers thick. For simplicity in comparing results with different zone thicknesses the radius was assumed to be 1700 kilometers.

Three major compositional phases whose concentrations can be specified as a function of depth are recognized: a high melting or "dunite" phase; a low melting or "basalt" phase; and a magma phase. Three minor elements are also

recognized: potassium, uranium, and thorium. The potassium and uranium concentrations are specified independently as a function of depth. The uranium to thorium ratio is held constant at 3.7.

The initial temperature, melting temperature and heat of fusion are specified as a function of depth, and the thermal conductivity is specified as a function of the local temperature.

For most minerals the specific heat increases as a function of temperature, however, we have taken a mean value of 1.1 joules/gram °K as representative over the range of interest. The heat of fusion also should be expected to vary with changes in the mineral assemblage present, again an average value, in this case 500 joules/gram has been chosen for the melting of the basaltic phase.

The melting temperature has been represented by the solidus for the Apollo basalts as determined by Ringwood and Essene (1970).

The two most uncertain thermal parameters in our calculations are the temperature distribution at the time of formation and the thermal conductivity. There is strong evidence that the surface of the moon was at or near melting at the time of formation and that the interior was relatively cooler, which has been attributed by some (Mitzutani, et.al., 1971; Wood, 1971) to differences in energy of accretion, a simple model for the initial temperature distribution was taken where the temperature in °K at radius r is approximated by the expression

$$T(r) = fE/c + 273$$

where: E is the accretional energy in joules/gram

c is the specific heat

f is the fraction of accretional energy retained.

For the purpose of this calculation E has been taken to be the energy of a particle arriving at the escape velocity appropriate to the particular radius, C to be 1.1 joules/gram, and f a constant .35, independent of depth.

The relevant initial and melting temperatures are shown in Figure 1.

Magma Migration

The main difference between these calculations and those of other calculations is the manner in which the movement of radioactive elements is tied directly to the movement of melt. Under the assumption that infinitesimal amounts of melt will not move to the surface, the program accepts as input the number of grams of melt per cubic centimeter that must remain at a given depth after extrusion has taken place. The program simulates extrusive activity by removing any excess melt from a partially molten zone and adding it to the surface layer. Solid material from above is then allowed to fall down and fill the space and the composition is adjusted accordingly.

For some of our early calculations liquid was allowed to remain in the zone above to block downward diffusion of radioactive elements concentrated in the melt. Unfortunately, this resulted in large concentrations of these elements at the bottom of the crust. After a while the concentration of heat sources there was so great that a continuous cycle of melting, extrusion, and remelting of the uppermost basaltic layers occurred. The resulting thermal profile

developed a large hump much like that appearing in Wood's (1970) calculations. Since this concentration effect seemed unrealistic, the procedure was altered so that solid was moved downward but the melt that would have been associated with it was tapped off and allowed to move to the surface.

The effects described above occurred when the radioactive elements were assumed to concentrate entirely in the melt. The computer program also allows one to chose two other ways to distribute the radioactivity; either evenly between the melt and solid basalt phases, or equally among the melt, solid basalt, and dunite phases. The results of thermal history calculations using the latter two options were described in considerable detail in McConnell, et.al. (1967), but they only have been utilized during the current study for test purposes. A flow chart for the entire thermal history program is shown in Figure 2.

Results of Calculations

A number of different models were tested during the course of program development. None of these have yet been found to produce results in accord with all the observations. Because there is no simple linear relationship between the observations and the input variables, the problem of finding a suitable model is still largely one of trail and error. We discuss below the results of several attempts to determine whether reasonable conditions, composition, and thermal properties can be expected to give rise to two separate periods of volcanism; the first occurring between 4.6×10^9 and 4.4×10^9 years B.P., and the second approximately 3.5 billion years B.P.

In all the models described below, the initial composition was taken to be 1.6 g/cc of the low melting or "basalt" phase and 1.7 g/cc of the high melting or "dunite" phase. The fraction of melt which must be present before extrusion can take place was set at .8 grams/cc, approximately one quarter of the total volume.

All models had a uranium concentration of .1 ppm at the surface which decreased to .018 ppm in the deep interior and a near surface potassium concentration of 150 ppm, which increased to 350 ppm below 600 km. (Figures 3, 4, 5) GM-4A and GM-4B are completely identical except that the former utilized the early version of the program discussed above which allowed a high concentration of radioactive melt to accumulate near the bottom of the crust, while GM-4B and GM-6 used the later version which eliminated this effect.

For GM-4A and GM-4B the thermal conductivity was taken to be .008 watts/cm °K. This value is very low for most basic and ultrabasic silicate rocks and roughly corresponds to the mean value of the synthetic lunar basalt reported by Murase & McBirney (1970). It was chosen as a lower bound for reasonable conductivities in order to test whether melting could occur under the most favorable conditions in an initially unmelted moon. In Model GM-6 the conductivity was doubled to .015 watts/cm °K, a more typical value for basalts. In both cases changes of temperature with conductivity were neglected.

Both versions of GM-4 predict volcanic activity beginning about 4.4×10^9 years B.P. and gradually decreasing until the present time. (Figure 6) The most recent activity is considerably more intense for GM-4A than for GM-4B as a result of the continual overturn of the crustal layers caused by the

concentration of radioactivity at the base of the solid crust. The improvement in GM-4B resulting from abandoning this feature is obvious. Unfortunately, neither of the above models shows a distinct break between the early melting period and the later one. One possible explanation for this is the relatively smooth variation in radioactive element concentrations as a function of depth which results in a continuous downward migration of the melting zone. To test this hypothesis a much sharper gradation in the uranium concentration was utilized in Model GM-6 (Figure 5). We also increased the thermal conductivity for this model to 0.015 watts/cm °K, since other tests had shown that the extremely low values were not necessary to induce early melting. As shown in Figure 6, GM-6 exhibits in a somewhat cleaner separation of the various periods of volcanic activity, but still not as distinct as indicated by field evidence. It is not yet possible to say whether a better selection of parameters can improve the predictions or whether it will ultimately be necessary to invoke other factors such as retention of the melt at depth until release is triggered by mare basin formation.

Among the more successful predictions of the three models is the minor element composition of the mare basalts. The K, U, and K/U values for the upper 20 kilometers at 3.5×10^9 years B.P. are shown in Table 1.

Table 1

Model	ppmK	ppmU	K/U
GM-4A	457	.256	1780
GM-4B	595	.333	1780
GM-6	381	.163	2340

All are sufficiently close to the observed values to be considered reasonable.

The present heat flow for the three models is shown in Table II.

Table II

Model	Conduction	Volcanic	Total
GM-4A	1.03	1.00	2.03
GM-4B	1.87	.37	2.24
GM-6	1.77	.46	2.23

As all show continuing volcanic activity at the present time the heat from the interior is thus transported via two mechanisms conduction and convection. The contribution of the volcanic heat to the flow measured by a lunar surface experiment is a strong function of the way the melt behaves when it reaches the surface and is not predictable from the model. The total heat flow however is relatively insensitive to the transport mechanism and it is this which should probably be used to compare predictions and observations. We note that the predicted values for all three models are about thirty percent lower than that measured by the Apollo 15 heat flow experiment, suggesting that higher radioactivity would provide a better fit. An alternative explanation is that a very high effective conductivity, perhaps due to solid state convection is causing the interior to cool rapidly at the present time. There is some doubt however as to whether this could provide a suitable explanation as the total heat flow is almost exactly equal to the present rate of production.

We turn now to the present temperature distributions (Figure 7). All models show internal temperatures which are much higher than those predicted by Sonnett, et.al. While the near surface values could be reduced by increasing the conductivity and/or the extent to which radioactive elements are concentrated in the crust, we find it difficult to see any mechanism for lowering the temperatures in the deep interior without a further drastic reduction in the original uranium concentration at depth.

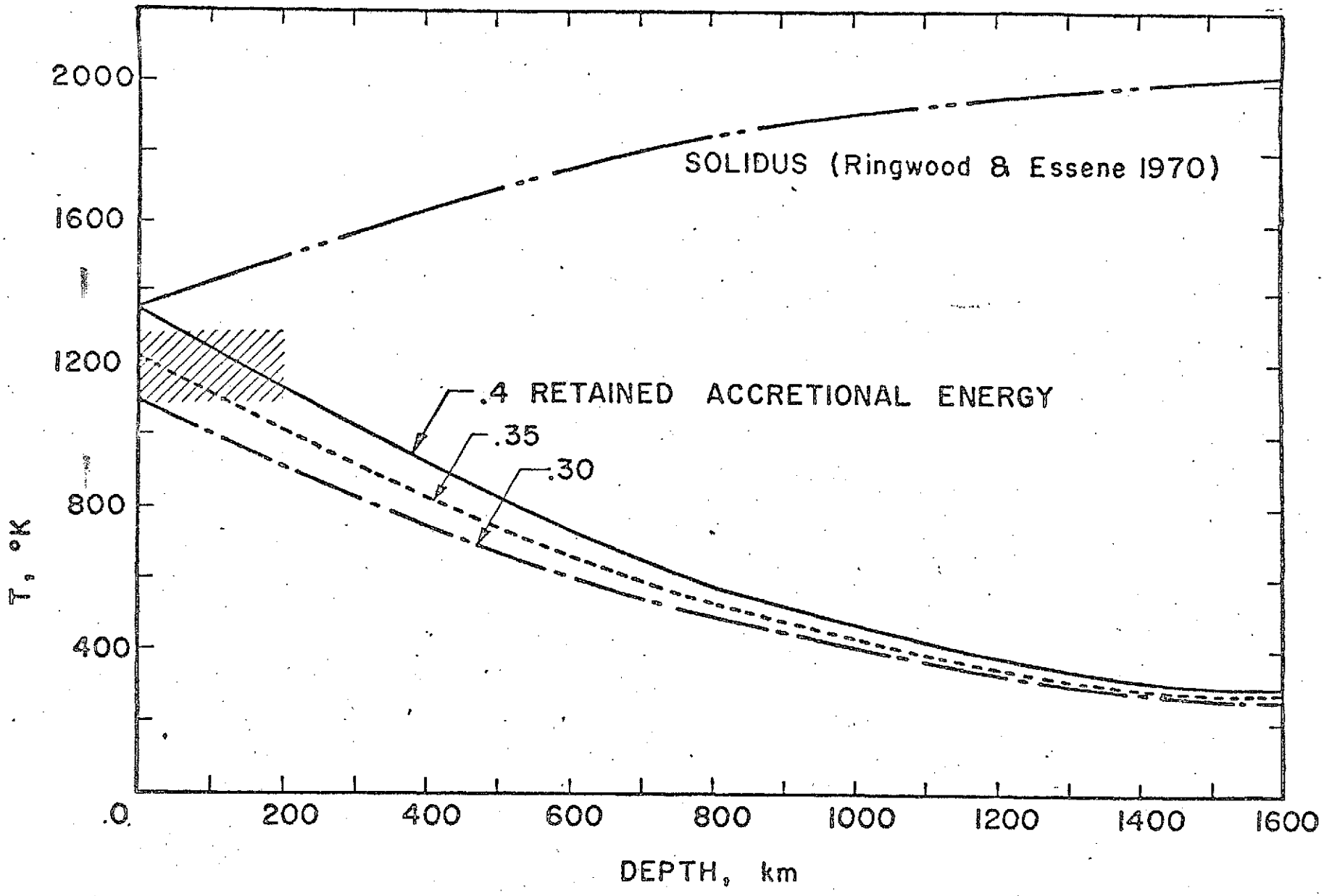
2000
1600
1200
800
400
T, °K
SOLIDUS (Ringwood & Essene 1970)
.4 RETAINED ACCRETIONAL ENERGY
.35
.30
0
200
400
600
800
1000
1200
1400
1600
DEPTH, km

FIGURE 1

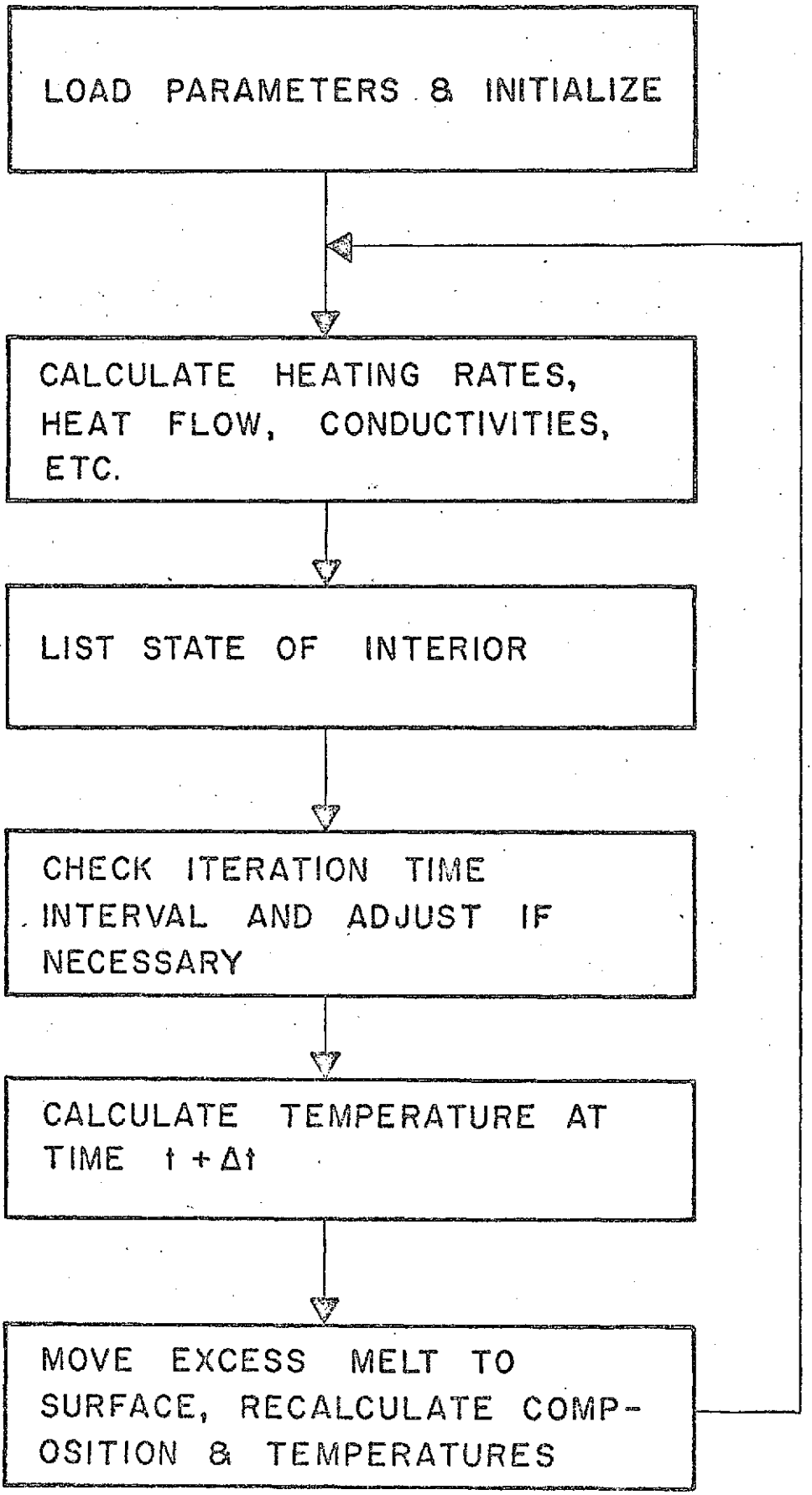
LOAD PARAMETERS & INITIALIZE
CALCULATE HEATING RATES, HEAT FLOW, CONDUCTIVITIES, ETC.
LIST STATE OF INTERIOR
CHECK ITERATION TIME INTERVAL AND ADJUST IF NECESSARY
CALCULATE TEMPERATURE AT TIME t + Δt
MOVE EXCESS MELT TO SURFACE, RECALCULATE COMP-OSITION & TEMPERATURES

FIGURE 2

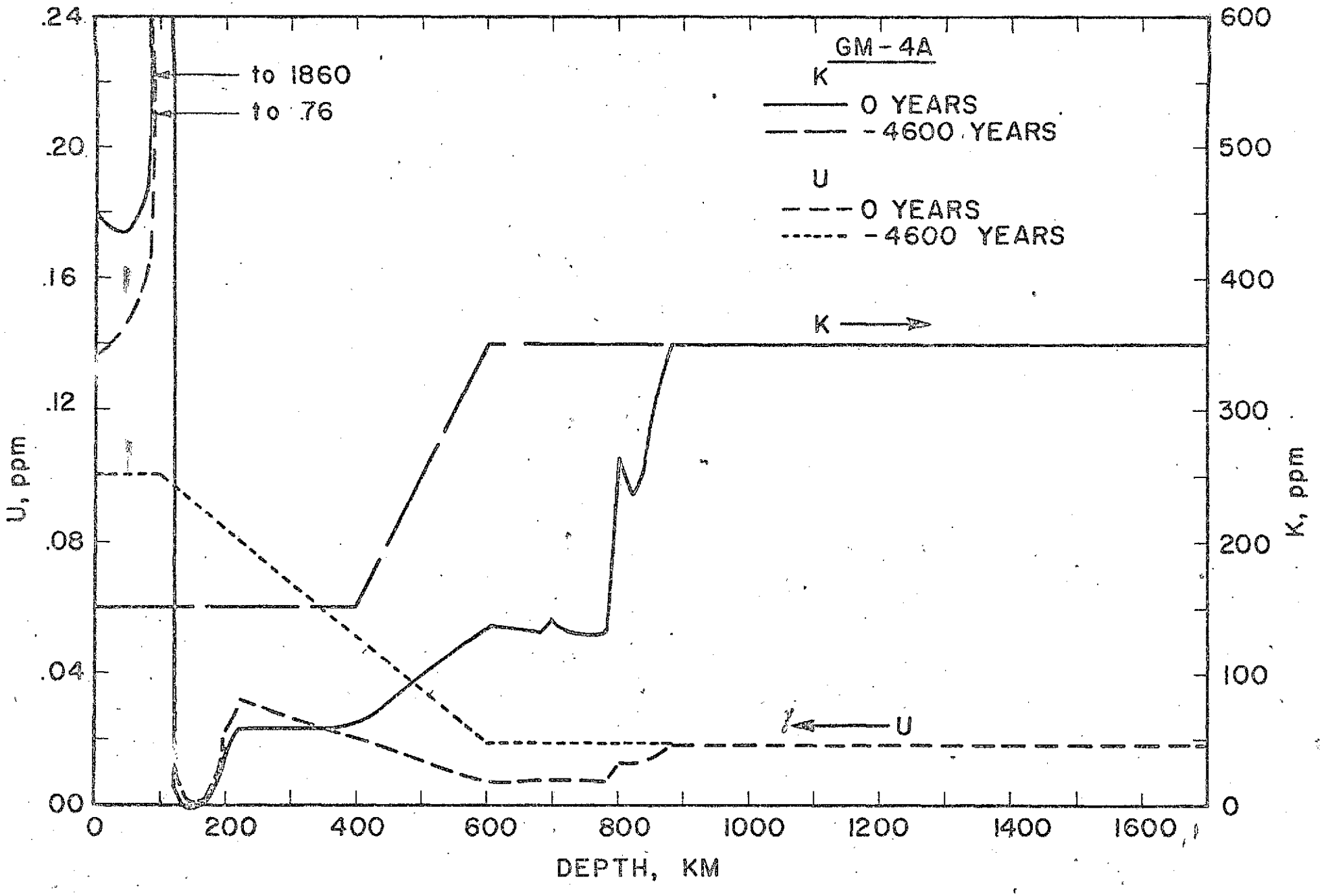
GM-4A
K
0 YEARS
-4600 YEARS
U
0 YEARS
-4600 YEARS
to 1860
to 76
K
U
U, ppm
K, ppm
DEPTH, KM
.24
.20
.16
.12
.08
.04
00
600
500
400
300
200
100
0
0
200
400
600
800
1000
1200
1400
1600

FIGURE 3

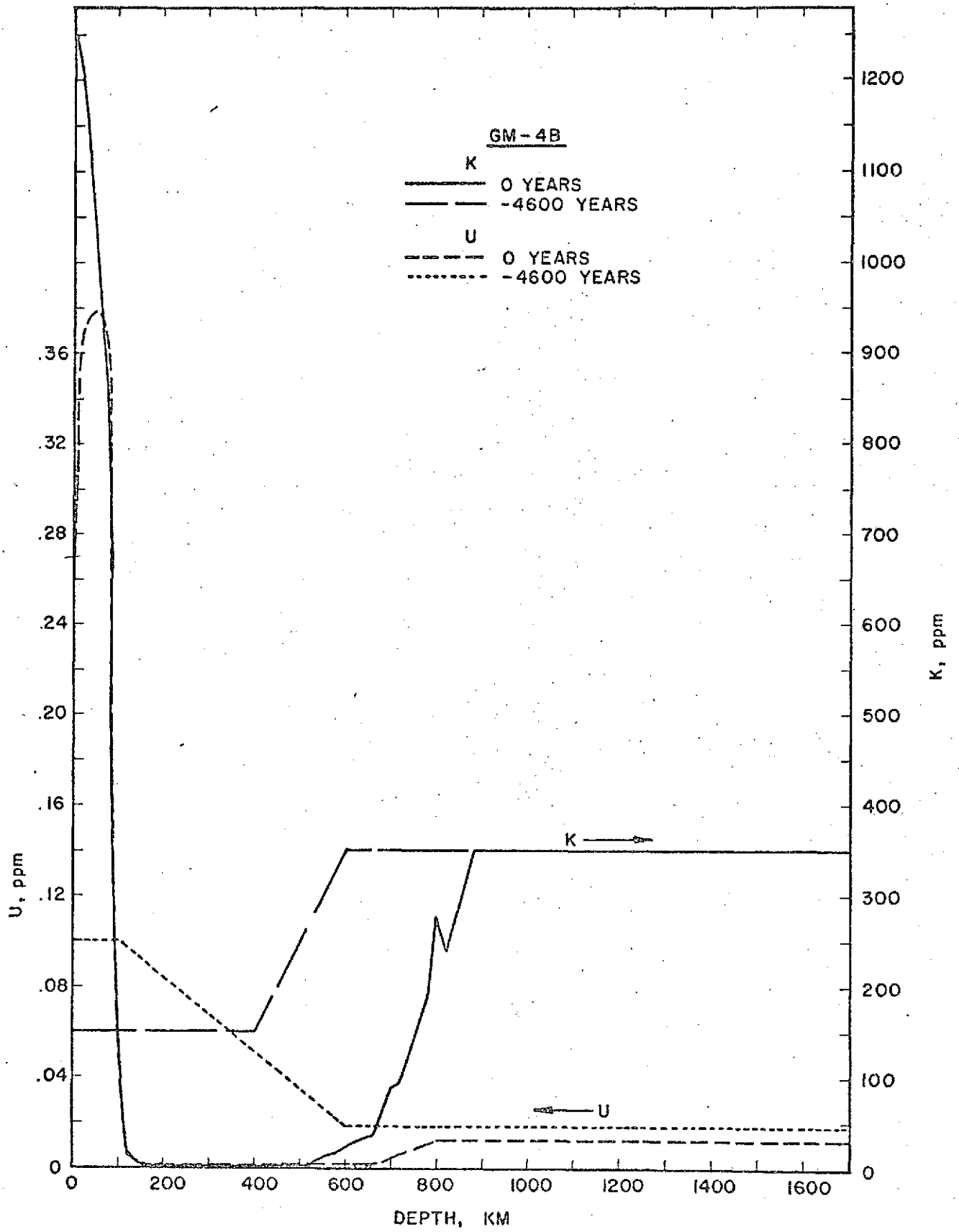
GM-4B
K
0 YEARS
-4600 YEARS
U
0 YEARS
-4600 YEARS
K
U
U, ppm
K, ppm
DEPTH, KM
0
.04
.08
.12
.16
.20
.24
.28
.32
.36
100
200
300
400
500
600
700
800
900
1000
1100
1200
0
200
400
600
800
1000
1200
1400
1600

FIGURE 4

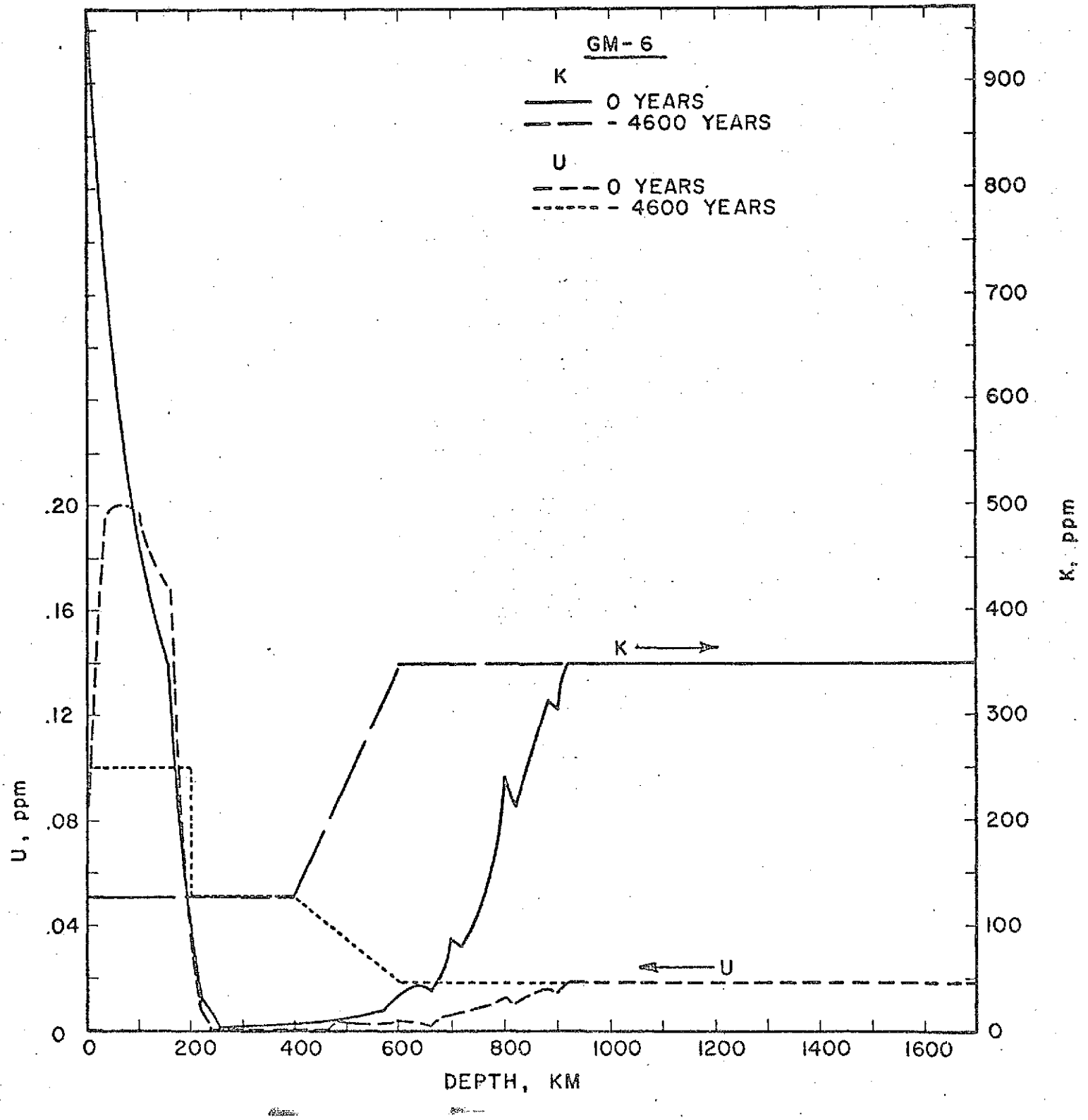
GM-6
K
0 YEARS
4600 YEARS
U
0 YEARS
4600 YEARS
K
U
U, ppm
K, ppm
DEPTH, KM
0
.04
.08
.12
.16
.20
100
200
300
400
500
600
700
800
900
0
200
400
600
800
1000
1200
1400
1600

FIGURE 5

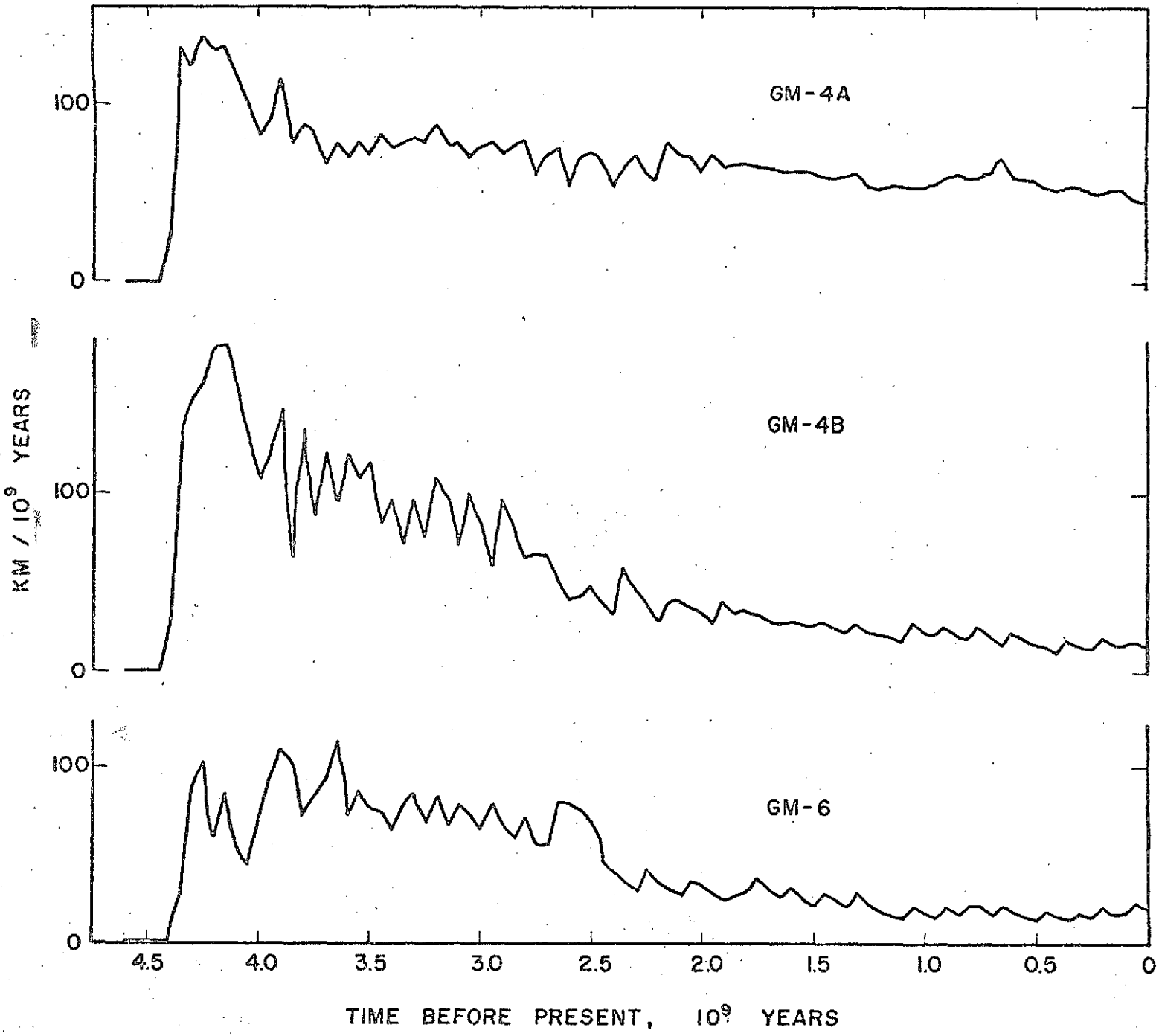
GM-4A
GM-4B
GM-6
100
0
KM / 10⁹ YEARS
4.5
4.0
3.5
3.0
2.5
2.0
1.5
1.0
0.5
0
TIME BEFORE PRESENT, 10⁹ YEARS

FIGURE 6

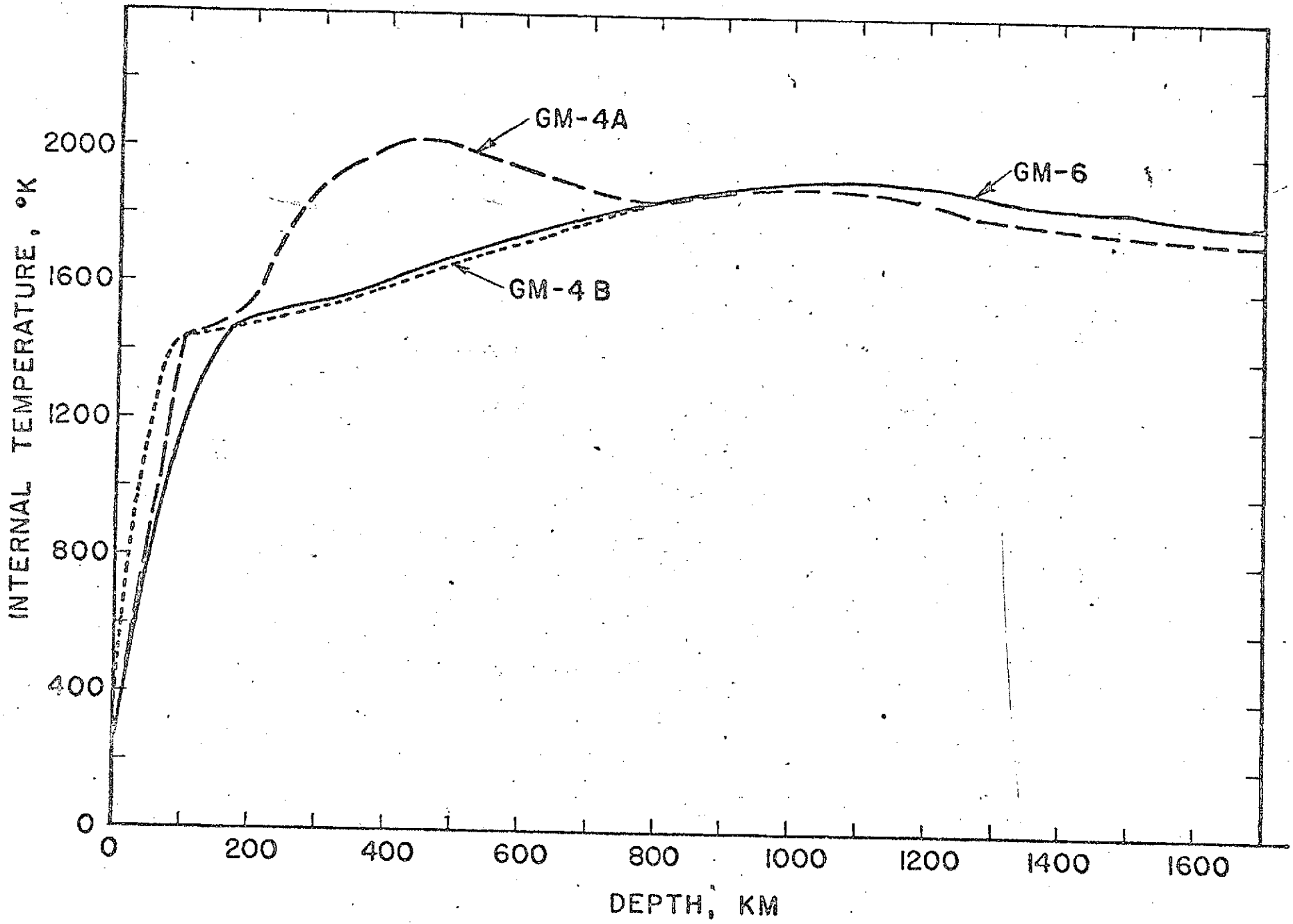
GM-4A
GM-6
GM-4 B
INTERNAL TEMPERATURE, °K
2000
1600
1200
800
400
0
0
200
400
600
800
1000
1200
1400
1600
DEPTH, KM

FIGURE 7

III. LUNAR MAGNETIC ANOMALY CALCULATIONS

During the Appolo program both surface magnetometers and subsatellite magnetometers indicated the presence of magnetic field anomalies on the moon. In order to test various hypotheses regarding the origin of these anomalies a variety of calculations were carries out using the numerical techniques developed by Talwani (1965).

We first tested the hypothesis that anomalies associated with lunar craters could be explained by uniformaly magnetized sheets of basalt with holes punched through them by impacts. Calculations were made of the horizontal and vertical field anomalies, as seen from a satellite passing directly over a crater at a height of 110 kilometers, for craters with radii of 50, 100, and 200 kilometers and thicknesses of 20, 40, and 100 kilometers. Three directions of magnetization were examined: vertical; horizontal parallel to the satellite path; and horizontal perpendicular to the satellite path. The results of these calculations are shown in Appendix 1.

To examine the surface anomalies at the Appolo 15 site a simplified map of the regions topography was drawn up and digitized (Figure 8). Because of the irregularity of the topography and the resulting problem of handling disconnected contours, considerable time was devoted to developing appropriate techniques and running test programs. Calculations were then made using a magnetization of 2×10^{-6} emu/gm. which indicate an anomaly of approximately 0.2 γ in the neighborhood of the LM. As a result of these calculations it

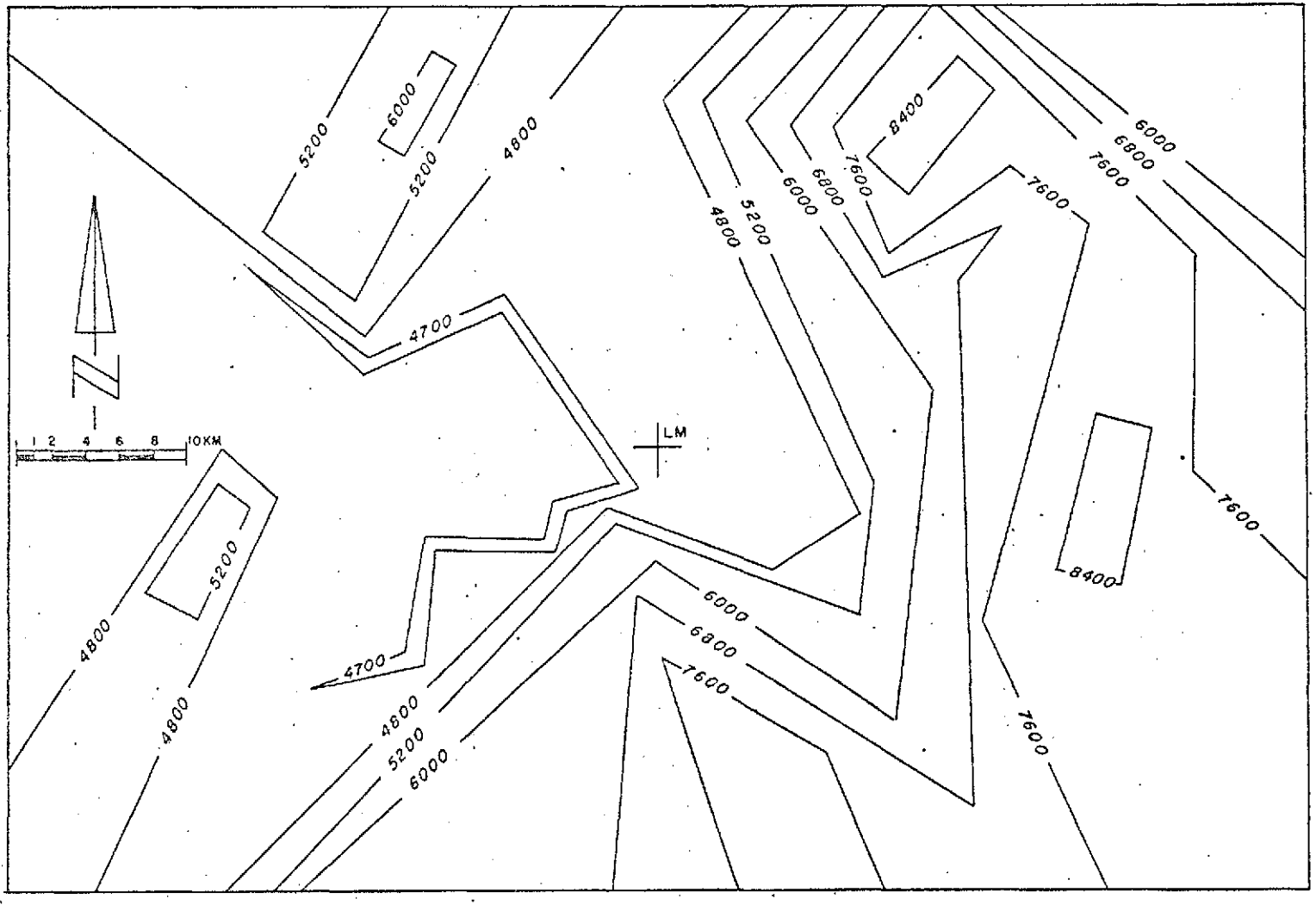

FIGURE 8 TOPOGRAPHIC MODEL FOR MAGNETIC CALCULATIONS – HADLEY REGION

was concluded that the anomaly at the landing site cannot be explained by rocks with magnetizations comparable to those sampled at the edge of the rille but can be explained by magnetizations which fall within the range of mare gasalt samples. This is discussed in more detail by Strangway et al. (1973).

The largest surface anomalies measured during the Appolo program occur at the Appolo 16 site where 5 readings fell between 121 and 313 gammas. To test the hypothesis that these anomalies are associated with the Cayley formation breccia flow, which fills the valley and which is known to have strong remanant magnetization, we computed the anomalies for a simplified model representing the edge of a basin filled with Cayley-like material. The results which indicate that a permanent magnetization of the order of 2×10^{-4} emu/gm. would account for the level of observed anomalies are reported in more detail in Strangway et al. (1973).

IV. SPECULATIONS ON THE RELATIONSHIPS BETWEEN THE THERMAL AND MAGNETIC HISTORY

The apparent paradox regarding the thermal evolution of the moon at the time the heat flow calculations were carried out can be summarized as follows:

1. Paleomagnetic studies of lunar basalts demonstrate that all such rocks returned to date were extruded at a time when the moon had a magnetic field.
2. In order to have a magnetic field the moon is assumed to have had a molten metallic core.
3. If the moon once had a deep molten core then it would still have one because of the low thermal conductivity.
4. Present measurements of the moon's internal temperature based on solar wind and seismic observations indicate that the interior is now relatively cool.
5. Therefore the moon could never have had a molten core.

The difficulty is to find a model warm enough to produce a mobile conducting layer and to melt basaltic rock and yet one which is cool enough in the deep interior to remain solid throughout the lunar history.

Except for the magnetic field paradox most other observational constraints can be fitted by a model which involves an initially differentiated moon enriched in refractory elements near the surface. The geochemical evidence

for such a model has been summarized by Gast (1972). If such a differentiated moon had the now widely accepted initial temperature distribution which was high near the surface and low in the interior it most likely began melting near the surface and the molten zone migrated downward as time wnet on (McConnell and Gast 1972). Typical rates of downward migration are .3 km per million years, i.e. 10^{-7} meters per second.

The molten zone would tend to accumulate high density components including such low viscosity conducting melts as metallic sulfides and metals. The importance of such a low viscosity layer is evident when one remembers that a molten core serves two purposes: first by being a highly conducting fluid it provides the physical environment necessary for generation of a magnetic field; secondly if the temperature gradient is superadiabatic convections will give rise to motions necessary for field generation.

It is important to note that convection is just one way of developing fluid motions necessary for field generation. Presumably any other mechanism which can produce appropriate velocity distributions would be equally good. We show below that if during the period of orbital evolution the moon was divided into two regions, a solid outer shell and an inner core, separated by a layer of molten conducting liquid of the order of tnes of kilometers thick then the core would tend to rotate differentially with respect to the shell. If the magnetic Reynolds number for the flow in the decoupling zone were high enough then magnetic field generation could be expected even though the bulk of the inner core remains cool.

To demonstrate the feasibility of this mechanism let us take an oversimplified lunar model consisting of a sphere with a uniform interior core of radius r_c and density ρ_c and an outer shell with sufficient gravitational dipole moment that remains oriented with one side aligned facing the earth. If we define (Figure 9)

Ω_s = angular velocity of shell relative to inertial space

Ω_c = angular velocity of core relative to inertial space

$\omega = \Omega_c - \Omega_s$

then

$$L_c \simeq \frac{d}{dt}\left[I_c\ (\Omega_s + \omega)\right] \quad . \tag{1}$$

where

L_c is the torque exerted on the core by the shell

I_c is the moment of inertia of the core

For a molten layer of thickness h and viscosity η the torque exerted on the core due to the differential rotation ω can easily be shown to be approximately

$$L_c \simeq \frac{-16}{3}\,\pi\,\eta\,r_c^{\,3}\left[\frac{r_c}{h} - 1\right]\ \omega \tag{2}$$

$$\simeq \frac{-16}{3}\,\pi\,\eta\,\frac{r_c^{\,4}}{h}\,\omega \tag{3}$$

Let us neglect the effects of changes in core size with time as a result of downward migration of the molten zone and concentrate on the relationship between the orbital changes and ω.

Substituting the moment of inertia for the core

$$I_c = 8 \pi \rho r_c^{5/15} \tag{4}$$

and (2) into (1) yields the equation of motion

$$\frac{\dot{\omega}}{\Omega_s} + \frac{10}{\rho} \frac{\eta}{r_c^2} \left(\frac{r_c}{h} - 1 \right) \frac{\omega}{\Omega_s} + \frac{\dot{\Omega}}{\Omega_s} = 0 \tag{5}$$

which can be integrated numerically if $\dot{\Omega}_s/\Omega_s$ is known.

For the sake of the present discussion let us assume that for the period with which we are concerned the moon was in an approximately circular orbit with the shell aligned towards the earth so that

$$\Omega_s = \left(\frac{GM}{R^3} \right)^{1/2} = 2.0 \times 10^7 R^{-3/2} \tag{6}$$

where

G is the gravitational constant = 6.67×10^{-11} Nm/kg^2

M is the mass of the earth = 5.98×10^{24} kg

R is the radius of the moon's orbit

If the torque acting on the moon is related to the radius by an expression of the form

$$L = k R^{-\alpha} = \frac{d}{dt} (m R^2 \Omega) \tag{7}$$

where

k is some constant

m is the mass of the moon

Ω is the orbital angular velocity

it can easily be shown that

$$\frac{\dot{\Omega}_s}{\Omega_s} = -\frac{3}{2}\frac{\dot{R}}{R} = -\frac{3[(R_2/R)^{\alpha+1/2} - (R_1/R)^{\alpha+1/2}]}{2(\alpha+1/2)(t_2-t_1)} \tag{8}$$

Here t_1 and t_2 are the times at which the moon was at radii R_1 and R_2 respectively.

Choosing

$\alpha = 6$ appropriate for torques due to earth-moon tidal interaction

$R_1 = 20$ earth radii

$R_2 = 60$ earth radii

$t_2 - t_1 = 4.5 \times 10^9$ years

$\rho_c = 3.3 \times 10^3$ kg/m^3

$\eta = 5 \times 10^{-4}$ kg/m sec, typical of molten iron

$\omega = \dot{\omega} = 0$ at $t = -4.5 \times 10^9$ years

we then integrate (5) to determine $\omega(t)$ for various layer thicknesses h. Having obtained ω we are now in a position to determine when, if at all, conditions were favorable for magnetic field generation.

One normally assumes that a combination of turbulent flow and a magnetic Reynolds number much greater than 1 is required for dynamo action.

For large Reynolds numbers flow between rotating cylinders is unstable when

$$\Omega_s(r_c + h)^2 < \Omega_c(r_c)^2 \tag{9}$$

(Landau and Lifshitz 1959 p.108). If we assume that the same rule is valid for flow between spheres, substitute $\Omega_c = \Omega_s = \omega$ into (8) and rearrange we get as a criterion for instability

$$\beta \equiv \frac{\omega}{\Omega_s} \qquad \frac{2\ell}{r_c} + \frac{\ell^2}{r_c} \quad > \quad 1 \tag{10}$$

The magnetic Reynolds number is defined as

$$Re_m = \ell v \mu \sigma \tag{11}$$

where

ℓ is a characteristic length

v is a characteristic velocity

μ is the magnetic permeability

σ is the electrical conductivity

For this particular problem we may take

$\mu = 4\pi \times 10^{-7}$ webers/m^2

$\sigma = 3 \times 10^5$ mhos/m and

$\ell v = h(\Omega_s r_s - \Omega_c r_c)$

which simplifies to

$$Re_m = .38(\Omega_s h^2 - \omega h r_c) \tag{12}$$

For the moon dynamo the ratio of viscous Reynolds number to the magnetic Reynolds number: $\rho/\eta\mu\sigma \gg 1$

Computed values of β as a function of time for $h = 10$ km and $h = 20$ km are shown if Figure 10. Values of Re_m are of the order of 10^5 during the unstable period. Although $h = 20$ km would appear to give the best fit to the observations, it should also be pointed out that lower viscosities, which might be more appropriate for sulfides, would have the same effect.

One must also remember that (5) is valid only for laminar flow and that the onset of instability will give rise to increased viscous drag and drag induced by the build up of the magnetic field. The net result of this will probably be to stabilize the system at a value of β approximately equal to 1 rather than allowing it to overshoot as shown in Figure 10.

We therefore conclude that if a conducting layer with low enough viscosity to effectively decouple the core and outer shell is formed beneath the surface of the moon then conditions favorable to magnetic field generation will arise as a result of the normal orbital evolution and that much of the reason for the hot versus cold moon controversy no longer exists.

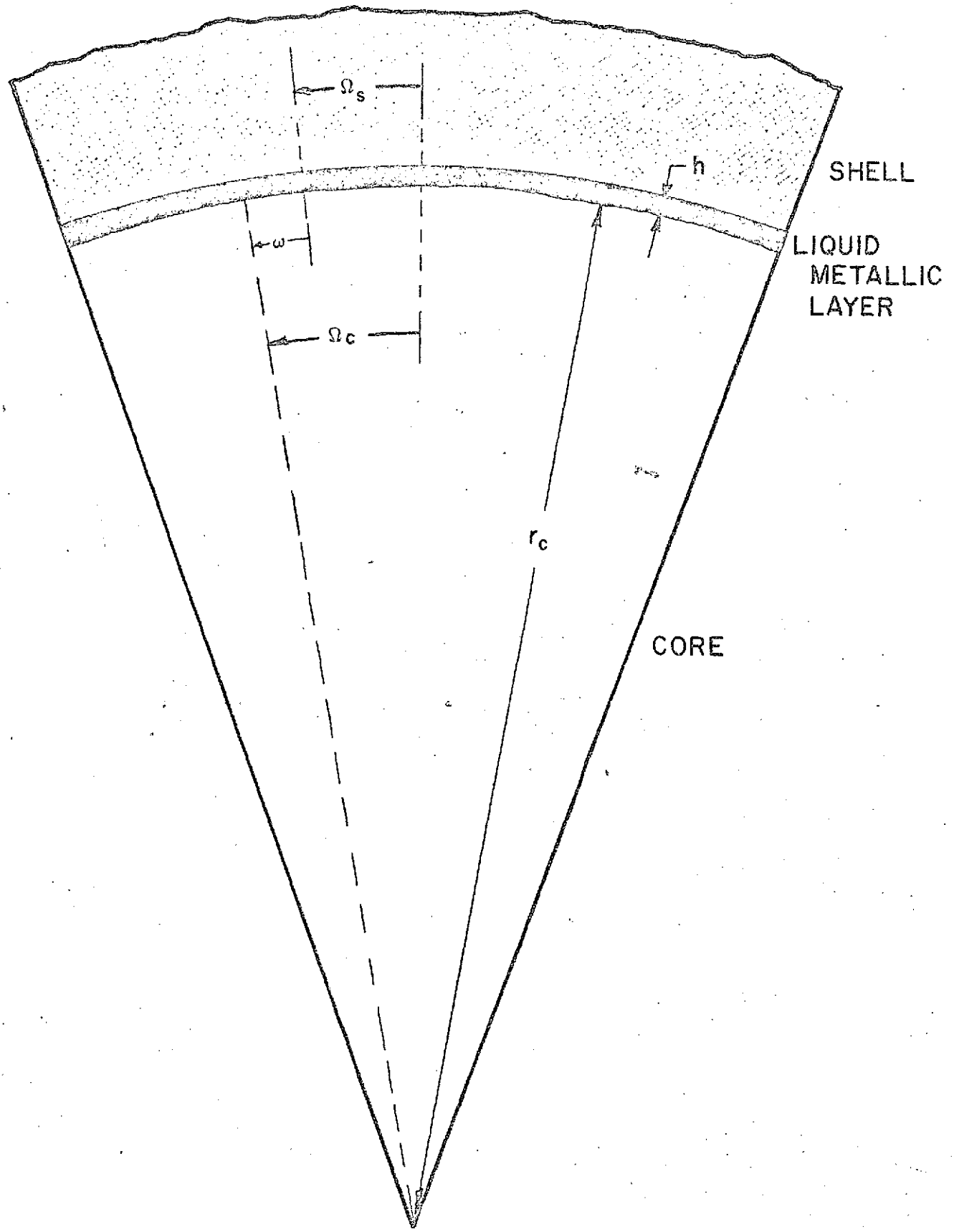

FIGURE 9

FIGURE 10

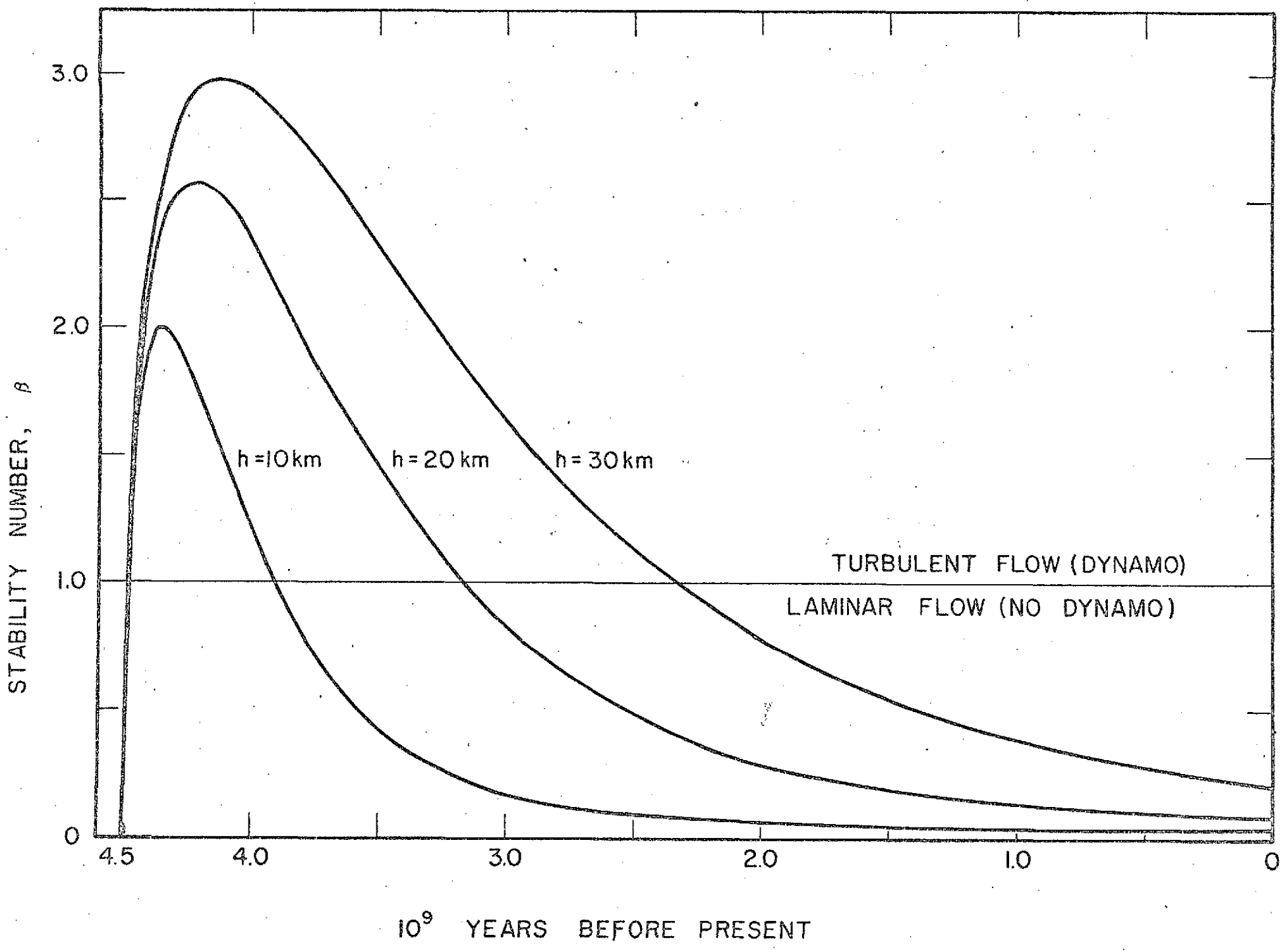
3.0
2.0
1.0
0
STABILITY NUMBER, β
h = 10 km
h = 20 km
h = 30 km
TURBULENT FLOW (DYNAMO)
LAMINAR FLOW (NO DYNAMO)
4.5
4.0
3.0
2.0
1.0
0
10⁹ YEARS BEFORE PRESENT

V. SUMMARY AND CONCLUSIONS

On the basis of the calculations discussed in the preceeding chapters we conclude that a realistic computer simulation of the evolution of the moon can be used to predict many more observables than heat flow and internal composition. These observables include major and minor element concentrations, thickness of the lunar "crust", intensity of volcanic activity as a function of time, etc.

The models which are most consistant with the observations include the following features:

1. A high surface temperature and low interior temperature during the very early lunar history;
2. High near surface radioactivity and relatively low radioactivity in the interior;
3. A molten zone formed at or near the surface which gradually migrates downward with time.

The lunar magnetic anomaly calculations demonstrate that the large anomalies measured at some of the landing sites and above some points on the surface cannot be caused by mare basalts but are consistant with valley fillings of Cayley-like material with a remnant magnetization of about 2×10^{-4} emu/gm.

We also speculate that the source of the magnetic field which must have been present in the early stages of lunar evolution could have been caused by a layer of conducting fluid at a depth of several hundred kilometers which acted to decouple the solid core from a solid crust.

REFERENCES

Aronson, J.R., L.H. Bellotti, S.W. Eckroad, A.G. Emslie, R.K. McConnell, and P.C. von Thuna, Infrared spectra and rediative thermal conductivity of m minerals at high Temperatures, A.D. Little, Inc., J. Geophys. Res., 75, 3443-3454, 1970.

Aronson, J.R., S.W. Eckroad, A.G. Emslie, R.K. McConnell, and P.C. von Thuna, Radiative thermal conductivity in planetary interiors, Nature, 216, 1096-10-97, 1967b.

Fricker, P.E., R.K. Reynolds, and A.L. Summers, On the thermal history of the moon, J. Geophy. Res., 72, 2649-2663, 1967.

Gast, P.W., The chemical composition of the earth, the moon, and chondritic meteorites, prepring, 1971a.

Gast, P.W., The chemical composition and structure of the moon, The Moon, Vol. 5, pp 121-148, 1972.

Hays, J.F. Radioactive heat sources in the lunar interior, unpublished paper, Department of Geological Sciences, Hoffman Laboratory, Harvard University, Cambridge, Mass., 1971.

Kaula, W.M., Interpretation of lunar mass concentrations, Phys. Earth Planet Interiors, 2, 123, 1969.

Landau, L.D., and E.M. Lifshitz, Fluid Mechanics , pp. 536, Pergamon Press, 1959.

Langseth, M.E., The appolo 15 lunar heat flow measurement, paper presented at the Lunar Science Institute Conference on Lunar Geophysics, Oct. 18-21, 1971, Houston, Texas.

McConnell, R.K., L.A. McClaine, D.W. Lee, J.R. Aronson, and R.V. Allen, A model for planetary igneous differentiation, Rev. Geophys., 5, 121-172, 1967.

McConnell, R.K. and P.W. Gast, Lunar thermal history revisited, The Moon, Vol. 5 pp 41-41, 1972

Mizutani, Hitoshi, Matui, T., Takeuchi, H., Accretional process of the moon, paper presented at the Lunar Science Institute Conference on Lunar Geophysics, Houston, Texas, Oct., 18-21, 1971.

Murase, Tsutomu, A.R. McBirney, Thermal conductivity of lunar and terrestrial igneous rocks in their melting range, (abstract), Science, 170, 165-167, 1971.

Ringwood, A.E., and E. Essene, Petrogenesis of Apollo 11 basalts, internal constitution and origin of the moon, Geochim, Cosmochim, Acta, Suppl. 1, 34, 769, 1970.

Strangway, et al, Lunar Magnetic Anomalies and the Cayley Formation, Nature, Vol. 246, pp 112-115, 1973.

Talwani, Manik, Computation with the Help of a Digital Computer of Magnetic Anomalies Caused by Bodies of Arbitrary Shape, Geophysics, p. 797, vol. 30, no.5, 1965.

Toksoz, M.N., S. Solomon, J. Minear, D. Johnston, Thermal Evolution of the moon, paper presented at the Lunar Science Institute Conference on Lunar Geophysics, Houston, Texas, October 18-21, 1971.

Tozer, D.C., An Interpretation of the lunar electrical conductivity distribution, paper presented at the Lunar Science Institute Conference on Lunar Geophysics, Houston, Texas, October 18-21, 1971.

Wook, J.A., Thermal history and early magmatism in the moon, The Geophysical Interpretation of the Moon, Ed. Gene Simmons, in press, 1970.

MAGNETIC ANOMALIES OVER MODEL LUNAR CRATERS

It has been postulated that magnetic anomalies associated with lunar craters result from the edge effects from around a hole punched out of a uniformly magnetized basaltic crust. If this is the case the measured anomalies can be used to estimate the thickness of the crust and the direction of magnetization at the time of implacement. These values in turn impose important constraints on the thermal and volcanic history of the moon.

The Models

The anomaly due to uniformly magnetized sheet with a hole punched in it is assumed to be equivalent to that of a disc of the same size as the hole with equal but opposite magnetization. For the purpose of the calculations such a disc is approximated by a regular sixteen sided polygon and the anomaly calculated using the method of Talwani (1965).

We have calculated anomalies for a variety of crater sizes, slab thicknesses, and magnetization directions in order to determine the main features of such anomaly patterns. For a coordinate system with origin at the top of the slab in the center of the crater the anomaly field components ΔX, ΔY, and ΔZ were calculated along the positive x axis out to the distance of 400 kilometers for the following models:

Satellite height - 110 kilometers
Crater radius - 50, 100, and 200 kilometers
Slab thickness - 20, 40, and 100 kilometers
Magnetization - No susceptibility effects
- Remnant intensity 10^{-5} emu/cc
- Remnant direction - horizontal parallel to satellite path
- horizontal perpendicular to satellite path
- vertical

Presentation of Results

The results of the calculations are given in the accompanying tables and figures.

For each crater three tables have been calculated, one for each direction of magnetization. With suitable transformations these can be used in conjunction with a desk electronic calculator to estimate the anomaly for any other field orientation or position over the crater.

Two graphs are also shown. The first presents the anomaly for the two horizontal magnetization directions as follows:

1. For the slab with the magnetization $\vec{J}$ parallel to the x axis the ΔX and ΔZ components are indicated by ⟶ and ↓ respectively. $\Delta Y = 0$ and is not shown.

2. When the magnetization is parallel to the y axis only the ΔY component is non-zero. This is indicated by ⊙ .

The second graph shows the anomalies for vertical magnetization with:

ΔX indicated by ⟶ ;
ΔY which is equal to zero, indicated by ⊙ ;
ΔZ indicated by ↓ .

SATELLITE HT. = 110 Km
RADIUS = 50 Km
DEPTH = 20 Km

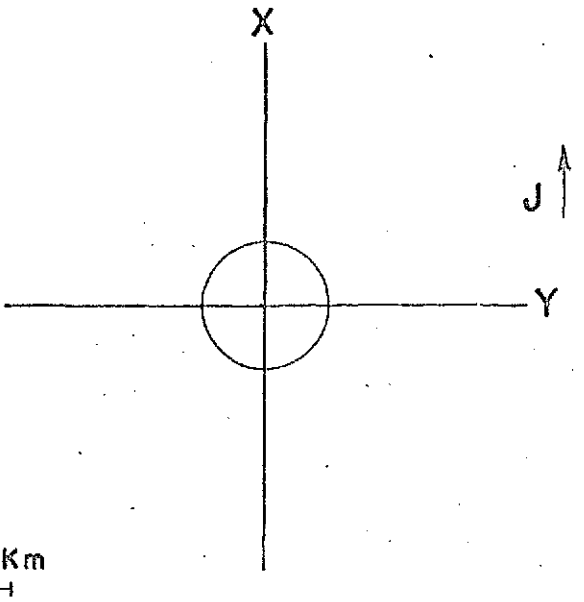

CRATER

MAGNETIZATION

INTENSITY = 10^{-5} emu
DECLINATION = 0.0 deg
INCLINATION = 0.0 deg

SATELLITE POSITION

x	y
0.0	0.0
20.00	0.0
40.00	0.0
60.00	0.0
80.00	0.0
100.00	0.0
120.00	0.0
140.00	0.0
160.00	0.0
180.00	0.0
200.00	0.0
220.00	0.0
240.00	0.0
260.00	0.0
280.00	0.0
300.00	0.0
320.00	0.0
340.00	0.0
360.00	0.0
380.00	0.0
400.00	0.0

ANOMALY

ΔX	ΔY	ΔZ
-0.073	0.000	-0.000
-0.067	-0.000	-0.030
-0.050	0.000	-0.053
-0.029	0.000	-0.064
-0.010	0.000	-0.064
0.004	0.000	-0.056
0.012	0.000	-0.046
0.016	-0.000	-0.037
0.016	0.000	-0.028
0.016	-0.000	-0.022
0.014	-0.000	-0.016
0.013	-0.000	-0.013
0.011	-0.000	-0.010
0.010	-0.000	-0.008
0.008	0.000	-0.006
0.007	0.000	-0.005
0.006	0.000	-0.004
0.005	0.000	-0.003
0.005	0.000	-0.003
0.004	-0.000	-0.002
0.004	0.000	-0.002

SATELLITE HT. = 110 Km
RADIUS = 50 Km
DEPTH = 20 Km

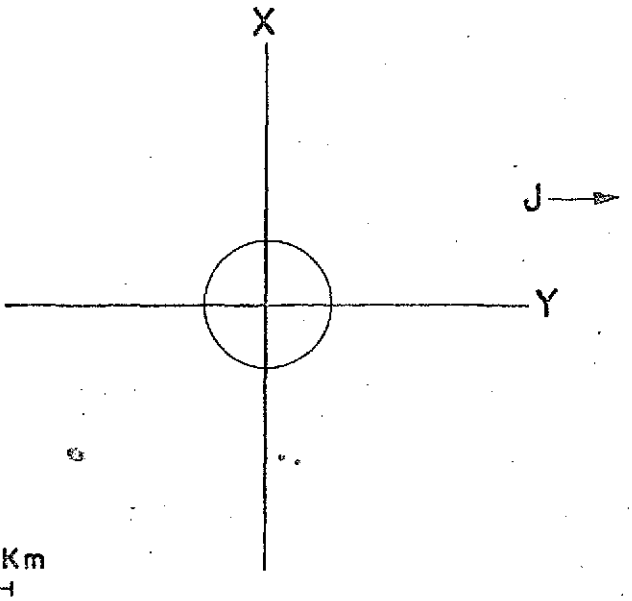

MAGNETIZATION

INTENSITY = 10^{-5} emu
DECLINATION = 90.0 deg
INCLINATION = 0.0 deg

CRATER

SATELLITE POSITION

x	y
0.0	0.0
20.00	0.0
40.00	0.0
60.00	0.0
80.00	0.0
100.00	0.0
120.00	0.0
140.00	0.0
160.00	0.0
180.00	0.0
200.00	0.0
220.00	0.0
240.00	0.0
260.00	0.0
280.00	0.0
300.00	0.0
320.00	0.0
340.00	0.0
360.00	0.0
380.00	0.0
400.00	0.0

ANOMALY

ΔX	ΔY	ΔZ
-0.000	-0.073	0.000
-0.000	-0.071	0.000
0.000	-0.065	0.000
0.000	-0.057	0.000
0.000	-0.047	0.000
0.000	-0.038	-0.000
0.000	-0.030	0.000
0.000	-0.024	-0.000
0.000	-0.019	-0.000
-0.000	-0.015	0.000
-0.000	-0.012	0.000
-0.000	-0.010	0.000
-0.000	-0.008	0.000
-0.000	-0.007	-0.000
0.000	-0.005	0.000
0.000	-0.005	0.000
0.000	-0.004	0.000
0.000	-0.003	0.000
0.000	-0.003	0.000
-0.000	-0.002	0.000
0.000	-0.002	0.000

SATELLITE HT. = 110 Km
RADIUS = 50 Km
DEPTH = 20 Km

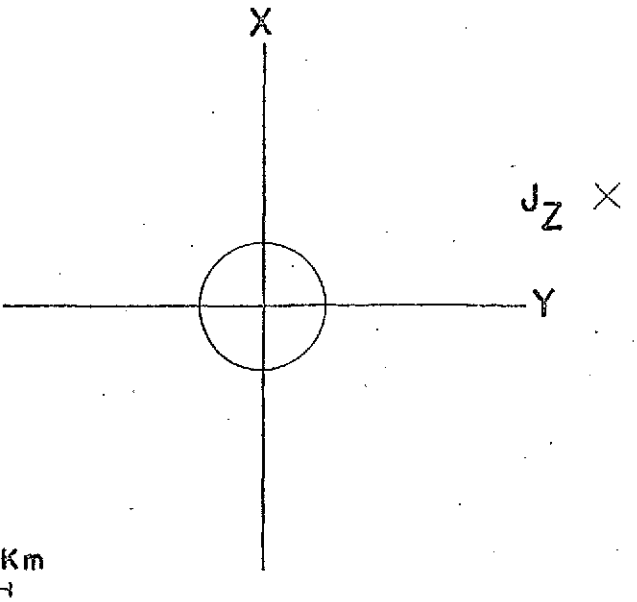

CRATER

MAGNETIZATION

INTENSITY = 10^{-5} emu
DECLINATION = 0.0 deg
INCLINATION = 90.0 deg

SATELLITE POSITION

x	y
0.0	0.0
20.00	0.0
40.00	0.0
60.00	0.0
80.00	0.0
100.00	0.0
120.00	0.0
140.00	0.0
160.00	0.0
180.00	0.0
200.00	0.0
220.00	0.0
240.00	0.0
260.00	0.0
280.00	0.0
300.00	0.0
320.00	0.0
340.00	0.0
360.00	0.0
380.00	0.0
400.00	0.0

ANOMALY

ΔX	ΔY	ΔZ
-0.000	0.000	0.147
-0.030	0.000	0.138
-0.053	0.000	0.115
-0.064	0.000	0.086
-0.064	0.000	0.057
-0.056	0.000	0.034
-0.040	0.000	0.018
-0.037	-0.000	0.008
-0.028	-0.000	0.003
-0.022	0.000	-0.001
-0.016	0.000	-0.002
-0.013	0.000	-0.003
-0.010	0.000	-0.003
-0.008	-0.000	-0.003
-0.006	0.000	-0.003
-0.005	0.000	-0.003
-0.004	0.000	-0.002
-0.003	0.000	-0.002
-0.003	0.000	-0.002
-0.002	0.000	-0.002
-0.002	0.000	-0.002

SATELLITE HT. = 110 Km
RADIUS = 50 Km
DEPTH = 40 Km

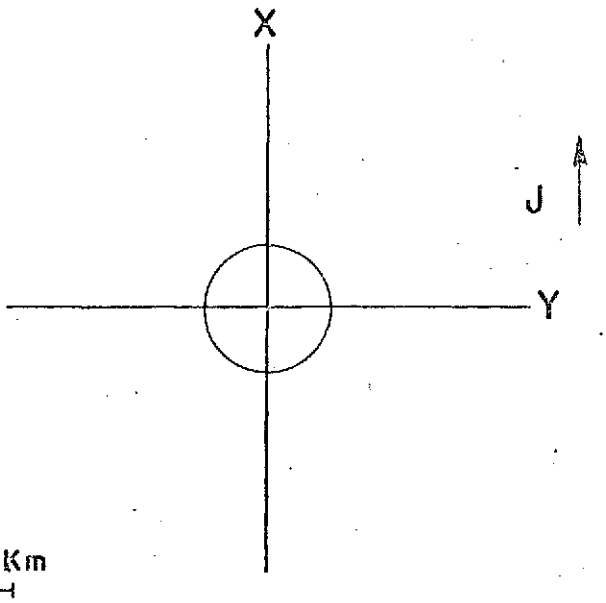

CRATER

MAGNETIZATION

INTENSITY = 10^{-5} emu
DECLINATION = 0.0 deg
INCLINATION = 0.0 deg

SATELLITE POSITION

x	y
0.0	0.0
20.00	0.0
40.00	0.0
60.00	0.0
80.00	0.0
100.00	0.0
120.00	0.0
140.00	0.0
160.00	0.0
180.00	0.0
200.00	0.0
220.00	0.0
240.00	0.0
260.00	0.0
280.00	0.0
300.00	0.0
320.00	0.0
340.00	0.0
360.00	0.0
380.00	0.0
400.00	0.0

ANOMALY

ΔX	ΔY	ΔZ
-0.133	0.000	-0.000
-0.122	-0.000	-0.055
-0.092	0.000	-0.096
-0.054	0.000	-0.115
-0.020	0.000	-0.115
0.005	0.000	-0.103
0.020	0.000	-0.086
0.027	-0.000	-0.068
0.029	-0.000	-0.053
0.028	-0.000	-0.041
0.026	-0.000	-0.032
0.023	0.000	-0.025
0.021	-0.000	-0.019
0.018	-0.000	-0.015
0.016	-0.000	-0.012
0.014	0.000	-0.010
0.012	0.000	-0.008
0.011	0.000	-0.006
0.009	0.000	-0.005
0.008	0.000	-0.004
0.007	0.000	-0.004

SATELLITE HT. = 110 Km
RADIUS = 50 Km
DEPTH = 40 Km

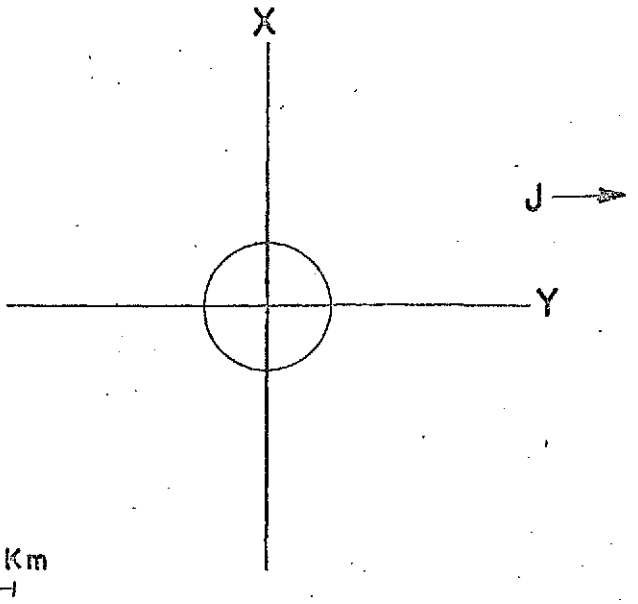

CRATER

MAGNETIZATION

INTENSITY = 10^{-5} emu
DECLINATION = 90.0 deg
INCLINATION = 0.0 deg

SATELLITE POSITION

x	y
0.0	0.0
20.00	0.0
40.00	0.0
60.00	0.0
80.00	0.0
100.00	0.0
120.00	0.0
140.00	0.0
160.00	0.0
180.00	0.0
200.00	0.0
220.00	0.0
240.00	0.0
260.00	0.0
280.00	0.0
300.00	0.0
320.00	0.0
340.00	0.0
360.00	0.0
380.00	0.0
400.00	0.0

ANOMALY

ΔX	ΔY	ΔZ
-0.000	-0.133	0.000
-0.000	-0.129	0.000
0.000	-0.119	0.000
0.000	-0.104	0.000
0.000	-0.087	0.000
0.000	-0.071	-0.000
0.000	-0.057	0.000
0.000	-0.045	-0.000
-0.000	-0.036	-0.000
-0.000	-0.029	0.000
-0.000	-0.023	0.000
0.000	-0.019	0.000
-0.000	-0.015	0.000
-0.000	-0.013	-0.000
-0.000	-0.011	0.000
0.000	-0.009	0.000
0.000	-0.008	0.000
0.000	-0.006	0.000
0.000	-0.006	0.000
0.000	-0.005	0.000
0.000	-0.004	0.000

SATELLITE HT. = 110 Km
RADIUS = 50 Km
DEPTH = 40 Km

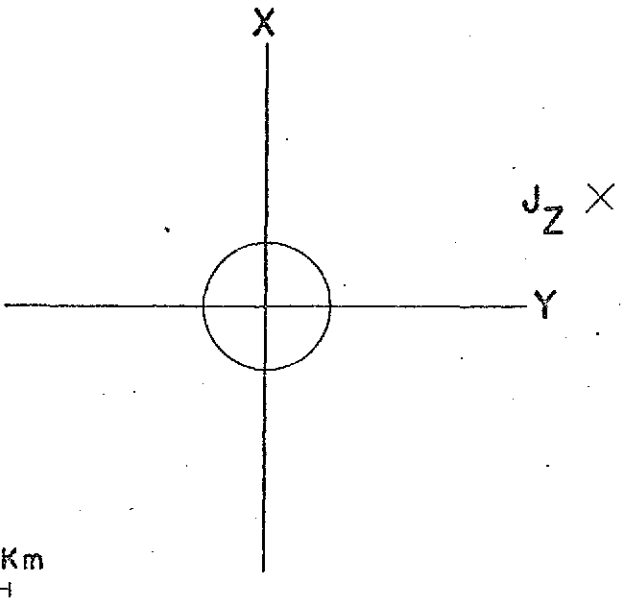

CRATER

MAGNETIZATION

INTENSITY = 10^{-5} emu
DECLINATION = 0.0 deg
INCLINATION = 90.0 deg

SATELLITE POSITION

x	y
0.0	0.0
20.00	0.0
40.00	0.0
60.00	0.0
80.00	0.0
100.00	0.0
120.00	0.0
140.00	0.0
160.00	0.0
180.00	0.0
200.00	0.0
220.00	0.0
240.00	0.0
260.00	0.0
280.00	0.0
300.00	0.0
320.00	0.0
340.00	0.0
360.00	0.0
380.00	0.0
400.00	0.0

ANOMALY

ΔX	ΔY	ΔZ
-0.000	0.000	0.267
-0.055	0.000	0.251
-0.096	0.000	0.211
-0.115	0.000	0.158
-0.115	0.000	0.106
-0.103	0.00	0.065
-0.086	0.000	0.037
-0.068	-0.000	0.018
-0.053	-0.000	0.007
-0.041	0.000	0.001
-0.032	0.000	-0.003
-0.025	0.000	-0.004
-0.019	0.000	-0.005
-0.015	-0.000	-0.005
-0.012	0.000	-0.005
-0.010	0.000	-0.005
-0.008	0.000	-0.004
-0.006	0.000	-0.004
-0.005	0.000	-0.004
-0.004	0.000	-0.003
-0.004	0.000	-0.003

SATELLITE HT. = 110 Km
RADIUS = 50 Km
DEPTH = 100 Km

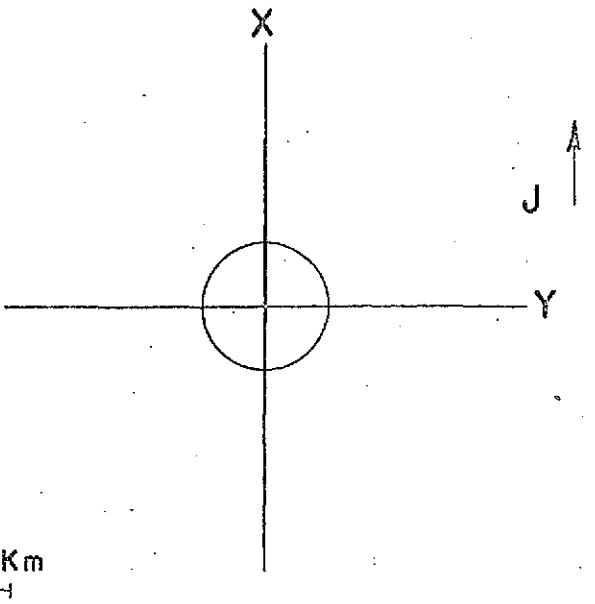

CRATER

MAGNETIZATION

INTENSITY = 10^{-5} emu
DECLINATION = 0.0 deg
INCLINATION = 0.0 deg

SATELLITE POSITION

x	y
0.0	0.0
20.00	0.0
40.00	0.0
60.00	0.0
80.00	0.0
100.00	0.0
120.00	0.0
140.00	0.0
160.00	0.0
180.00	0.0
200.00	0.0
220.00	0.0
240.00	0.0
260.00	0.0
280.00	0.0
300.00	0.0
320.00	0.0
340.00	0.0
360.00	0.0
380.00	0.0
400.00	0.0

ANOMALY

ΔX	ΔY	ΔZ
-0.317	-0.000	-0.000
-0.289	0.000	-0.132
-0.215	0.000	-0.229
-0.124	0.000	-0.274
-0.043	0.000	-0.271
0.015	-0.000	-0.239
0.047	0.000	-0.197
0.062	-0.000	-0.157
0.065	-0.000	-0.123
0.063	-0.000	-0.096
0.058	-0.000	-0.075
0.052	-0.000	-0.059
0.046	-0.000	-0.047
0.041	-0.000	-0.037
0.036	0.000	-0.030
0.032	-0.000	-0.025
0.028	0.000	-0.020
0.025	0.000	-0.017
0.022	0.000	-0.014
0.019	-0.000	-0.012
0.017	0.000	-0.010

SATELLITE HT. = 110 Km
RADIUS = 50 Km
DEPTH = 100 Km

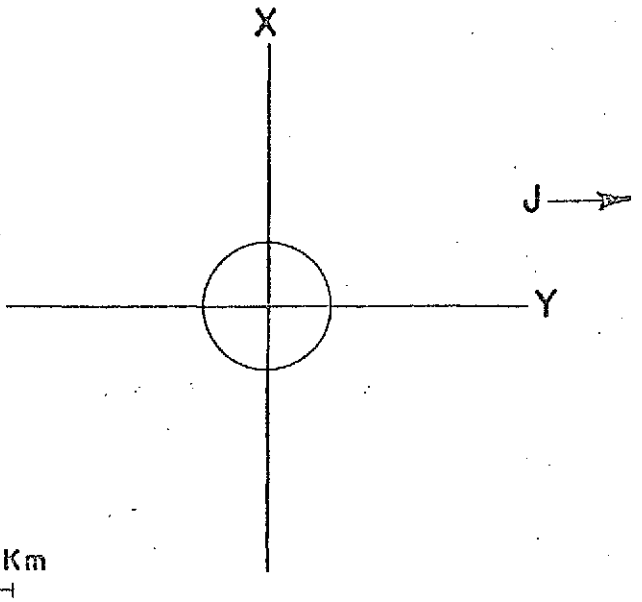

CRATER

MAGNETIZATION

INTENSITY = 10^{-5} emu
DECLINATION = 90.0 deg
INCLINATION = 0.0 deg

SATELLITE POSITION

x	y
0.0	0.0
20.00	0.0
40.00	0.0
60.00	0.0
80.00	0.0
100.00	0.0
120.00	0.0
140.00	0.0
160.00	0.0
180.00	0.0
200.00	0.0
220.00	0.0
240.00	0.0
260.00	0.0
280.00	0.0
300.00	0.0
320.00	0.0
340.00	0.0
360.00	0.0
380.00	0.0
400.00	0.0

ANOMALY

ΔX	ΔY	ΔZ
-0.000	-0.317	0.000
-0.000	-0.307	0.000
0.000	-0.281	0.000
0.000	-0.244	0.000
0.000	-0.203	0.000
-0.000	-0.165	-0.000
0.000	-0.132	0.000
-0.000	-0.105	-0.000
-0.000	-0.084	-0.000
-0.000	-0.068	0.000
-0.000	-0.055	0.000
0.000	-0.045	0.000
-0.000	-0.037	0.000
-0.000	-0.031	-0.000
0.000	-0.026	0.000
-0.000	-0.022	0.000
0.000	-0.019	0.000
0.000	-0.016	0.000
0.000	-0.014	0.000
-0.000	-0.012	0.000
0.000	-0.010	-0.000

SATELLITE HT. = 110 Km
RADIUS = 50 Km
DEPTH = 100 Km

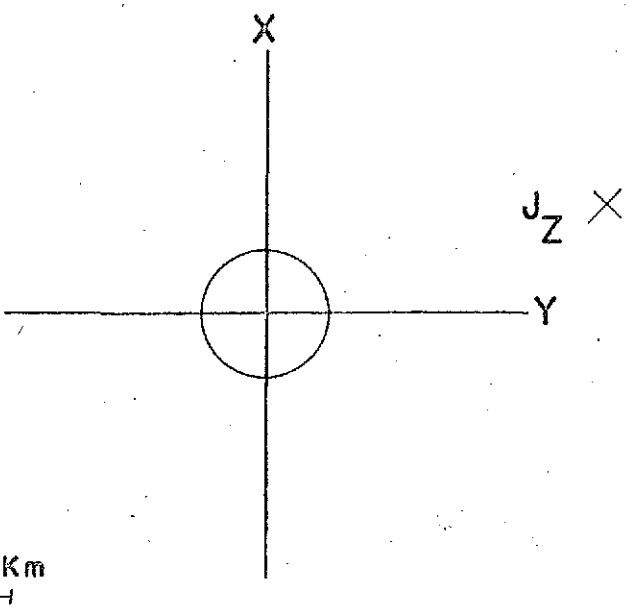

CRATER

MAGNETIZATION

INTENSITY = 10^{-5} emu
DECLINATION = 0.0 deg
INCLINATION = 90.0 deg

SATELLITE POSITION

x	y
0.0	0.0
20.00	0.0
40.00	0.0
60.00	0.0
80.00	0.0
100.00	0.0
120.00	0.0
140.00	0.0
160.00	0.0
180.00	0.0
200.00	0.0
220.00	0.0
240.00	0.0
260.00	0.0
280.00	0.0
300.00	0.0
320.00	0.0
340.00	0.0
360.00	0.0
380.00	0.0
400.00	0.0

ANOMALY

ΔX	ΔY	ΔZ
-0.000	0.000	0.633
-0.132	0.000	0.596
-0.229	0.000	0.496
-0.274	0.000	0.368
-0.271	0.000	0.246
-0.239	0.000	0.150
-0.197	0.000	0.085
-0.157	-0.000	0.043
-0.123	-0.000	0.019
-0.096	0.000	0.005
-0.075	0.000	-0.003
-0.059	0.000	-0.007
-0.047	0.000	-0.009
-0.037	-0.000	-0.010
-0.030	0.000	-0.010
-0.025	0.000	-0.010
-0.020	0.000	-0.009
-0.017	0.000	-0.009
-0.014	0.000	-0.008
-0.012	0.000	-0.007
-0.010	-0.000	-0.007

SATELLITE HT. = 110 Km
RADIUS = 100 Km
DEPTH = 20 Km

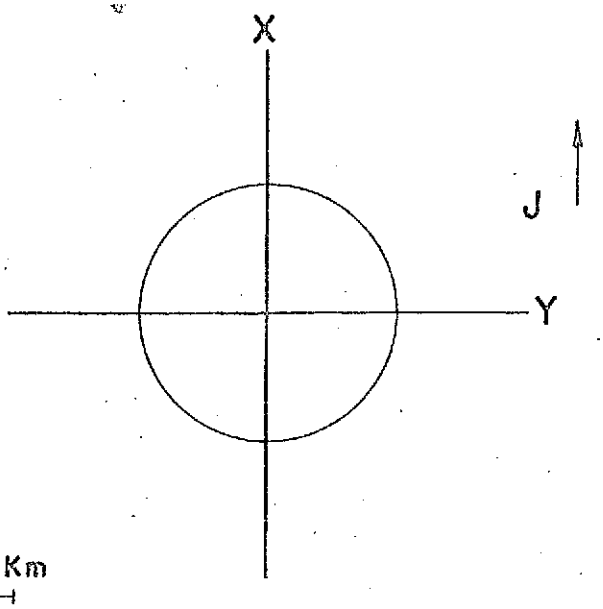

CRATER

MAGNETIZATION

INTENSITY = 10^{-5} emu
DECLINATION = 0.0 deg
INCLINATION = 0.0 deg

SATELLITE POSITION

x	y
0.0	0.0
20.00	0.0
40.00	0.0
60.00	0.0
80.00	0.0
100.00	0.0
120.00	0.0
140.00	0.0
160.00	0.0
180.00	0.0
200.00	0.0
220.00	0.0
240.00	0.0
260.00	0.0
280.00	0.0
300.00	0.0
320.00	0.0
340.00	0.0
360.00	0.0
380.00	0.0
400.00	0.0

ANOMALY

ΔX	ΔY	ΔZ
-0.167	0.000	0.000
-0.161	0.000	-0.049
-0.143	-0.000	-0.095
-0.113	0.000	-0.132
-0.075	0.000	-0.157
-0.035	0.000	-0.164
0.000	0.000	-0.156
0.026	0.000	-0.137
0.041	-0.000	-0.114
0.048	0.000	-0.091
0.048	0.000	-0.071
0.046	-0.000	-0.056
0.042	0.000	-0.043
0.037	0.000	-0.034
0.033	0.000	-0.027
0.029	0.000	-0.021
0.025	0.000	-0.017
0.022	0.000	-0.014
0.019	0.000	-0.011
0.017	0.000	-0.009
0.015	-0.000	-0.008

SATELLITE HT. = 110 Km
RADIUS = 100Km
DEPTH = 20 Km

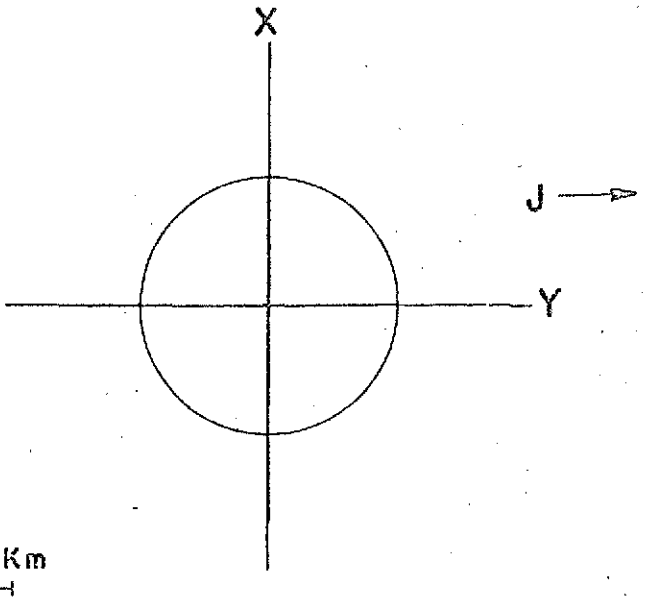

CRATER

MAGNETIZATION

INTENSITY = 10^{-5} emu
DECLINATION = 90.0 deg
INCLINATION = 0.0 deg

SATELLITE POSITION

x	y
0.0	0.0
20.00	0.0
40.00	0.0
60.00	0.0
80.00	0.0
100.00	0.0
120.00	0.0
140.00	0.0
160.00	0.0
180.00	0.0
200.00	0.0
220.00	0.0
240.00	0.0
260.00	0.0
280.00	0.0
300.00	0.0
320.00	0.0
340.00	0.0
360.00	0.0
380.00	0.0
400.00	0.0

ANOMALY

ΔX	ΔY	ΔZ
0.000	-0.167	0.000
0.000	-0.165	0.000
-0.000	-0.159	0.000
0.000	-0.149	0.000
0.000	-0.136	0.000
-0.000	-0.120	0.000
0.000	-0.102	0.000
0.000	-0.086	-0.000
-0.000	-0.071	0.000
0.000	-0.058	-0.000
0.000	-0.047	-0.000
-0.000	-0.039	-0.000
0.000	-0.032	0.000
0.000	-0.026	0.000
0.000	-0.022	0.000
0.000	-0.018	-0.000
0.000	-0.016	0.000
0.000	-0.013	0.000
0.000	-0.011	0.000
0.000	-0.010	0.000
-0.000	-0.009	0.000

SATELLITE HT. = 110 Km
RADIUS = 100 Km
DEPTH = 20 Km

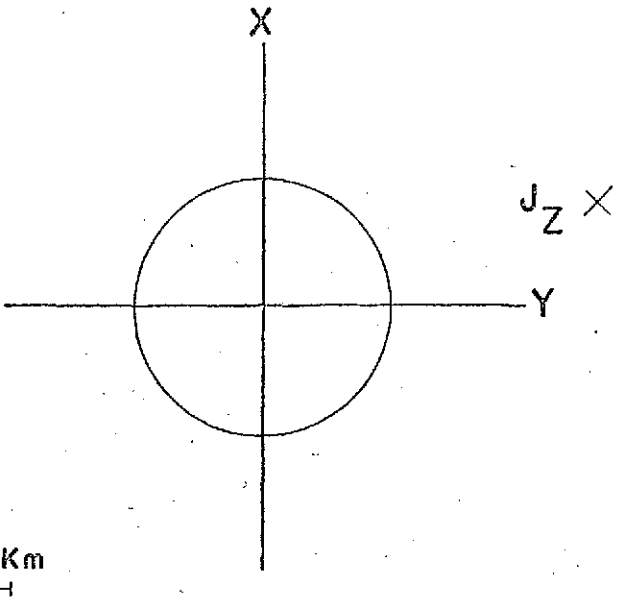

CRATER

MAGNETIZATION

INTENSITY = 10^{-5} emu
DECLINATION = 0.0 deg
INCLINATION = 90.0 deg

SATELLITE POSITION

x	y
0.0	0.0
20.00	0.0
40.00	0.0
60.00	0.0
80.00	0.0
100.00	0.0
120.00	0.0
140.00	0.0
160.00	0.0
180.00	0.0
200.00	0.0
220.00	0.0
240.00	0.0
260.00	0.0
280.00	0.0
300.00	0.0
320.00	0.0
340.00	0.0
360.00	0.0
380.00	0.0
400.00	0.0

ANOMALY

ΔX	ΔY	ΔZ
-0.000	0.000	0.335
-0.040	0.000	0.327
-0.095	0.000	0.302
-0.132	0.000	0.263
-0.157	0.000	0.211
-0.164	0.000	0.155
-0.156	0.000	0.102
-0.137	0.000	0.060
-0.114	0.000	0.030
-0.091	0.000	0.010
-0.071	-0.000	-0.001
-0.056	-0.000	-0.007
-0.043	0.000	-0.010
-0.034	0.000	-0.011
-0.027	0.000	-0.011
-0.021	0.000	-0.010
-0.017	0.000	-0.010
-0.014	0.000	-0.009
-0.011	0.000	-0.008
-0.009	0.000	-0.007
-0.008	0.000	-0.007

SATELLITE HT. = 110 Km
RADIUS = 100 Km
DEPTH = 40 Km

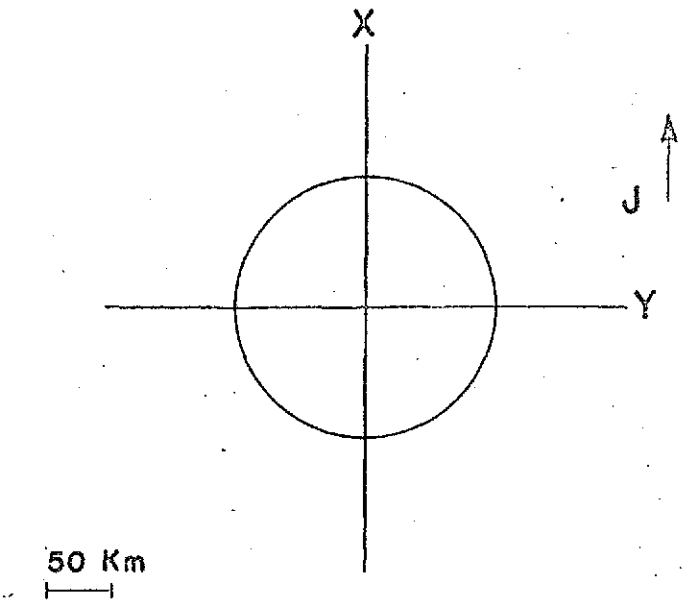

CRATER

MAGNETIZATION

INTENSITY = 10^{-5} emu
DECLINATION = 0.0 deg
INCLINATION = 0.0 deg

SATELLITE POSITION

x	y
0.0	0.0
20.00	0.0
40.00	0.0
60.00	0.0
80.00	0.0
100.00	0.0
120.00	0.0
140.00	0.0
160.00	0.0
180.00	0.0
200.00	0.0
220.00	0.0
240.00	0.0
260.00	0.0
280.00	0.0
300.00	0.0
320.00	0.0
340.00	0.0
360.00	0.0
380.00	0.0
400.00	0.0

ANOMALY

ΔX	ΔY	ΔZ
-0.309	0.000	0.000
-0.298	0.000	-0.090
-0.265	-0.000	-0.173
-0.211	0.000	-0.242
-0.143	0.000	-0.287
-0.069	0.000	-0.301
-0.004	0.000	-0.288
0.043	0.000	-0.254
0.071	-0.000	-0.213
0.084	0.000	-0.172
0.087	0.000	-0.137
0.083	-0.000	-0.108
0.077	-0.000	-0.085
0.069	0.000	-0.067
0.062	0.000	-0.053
0.054	0.000	-0.043
0.048	-0.000	-0.034
0.042	0.000	-0.028
0.037	0.000	-0.023
0.033	0.000	-0.019
0.029	-0.000	-0.016

SATELLITE HT. = 110 Km
RADIUS = 100 Km
DEPTH = 40 Km

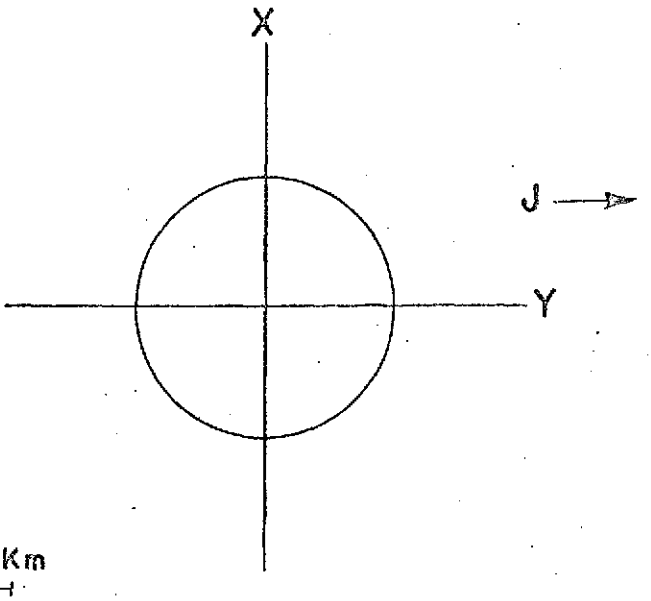

CRATER

MAGNETIZATION

INTENSITY = 10^{-5} emu
DECLINATION = 90.0 deg
INCLINATION = 0.0 deg

SATELLITE POSITION

x	y
0.0	0.0
20.00	0.0
40.00	0.0
60.00	0.0
80.00	0.0
100.00	0.0
120.00	0.0
140.00	0.0
160.00	0.0
180.00	0.0
200.00	0.0
220.00	0.0
240.00	0.0
260.00	0.0
280.00	0.0
300.00	0.0
320.00	0.0
340.00	0.0
360.00	0.0
380.00	0.0
400.00	0.0

ANOMALY

ΔX	ΔY	ΔZ
0.000	-0.309	0.000
0.000	-0.305	0.000
-0.000	-0.294	0.000
0.000	-0.276	0.000
0.000	-0.251	0.000
0.000	-0.222	0.000
0.000	-0.191	0.000
0.000	-0.161	-0.000
-0.000	-0.133	0.000
0.000	-0.110	0.000
0.000	-0.090	-0.000
-0.000	-0.074	-0.000
0.000	-0.061	0.000
0.000	-0.051	0.000
0.000	-0.043	0.000
0.000	-0.036	0.000
0.000	-0.031	0.000
0.000	-0.026	0.000
-0.000	-0.023	-0.000
0.000	-0.019	0.000
-0.000	-0.017	0.000

SATELLITE HT. = 110 Km
RADIUS = 100 Km
DEPTH = 40 Km

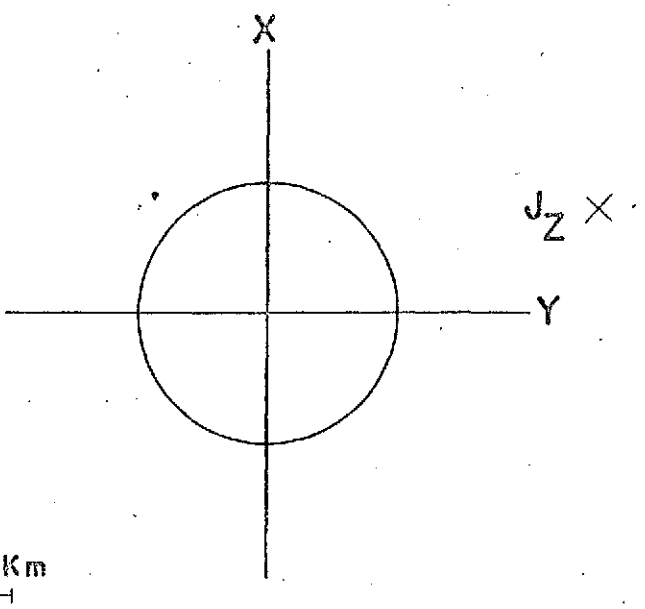

CRATER

MAGNETIZATION

INTENSITY = 10^{-5} emu
DECLINATION = 0.0 deg
INCLINATION = 90.0 deg

SATELLITE POSITION

x	y
0.0	0.0
20.00	0.0
40.00	0.0
60.00	0.0
80.00	0.0
100.00	0.0
120.00	0.0
140.00	0.0
160.00	0.0
180.00	0.0
200.00	0.0
220.00	0.0
240.00	0.0
260.00	0.0
280.00	0.0
300.00	0.0
320.00	0.0
340.00	0.0
360.00	0.0
380.00	0.0
400.00	0.0

ANOMALY

ΔX	ΔY	ΔZ
0.000	0.000	0.618
-0.090	0.000	0.603
-0.173	0.000	0.559
-0.242	0.000	0.487
-0.287	0.000	0.394
-0.301	0.000	0.292
-0.288	0.000	0.196
-0.254	0.000	0.118
-0.213	0.000	0.062
-0.172	0.000	0.026
-0.137	-0.000	0.004
-0.108	-0.000	-0.009
-0.085	0.000	-0.015
-0.067	0.000	-0.018
-0.053	0.000	-0.019
-0.043	0.000	-0.018
-0.034	0.000	-0.017
-0.028	0.000	-0.016
-0.023	0.000	-0.015
-0.019	0.000	-0.014
-0.016	0.000	-0.012

SATELLITE HT. = 110 Km
RADIUS = 100 Km
DEPTH = 100 Km

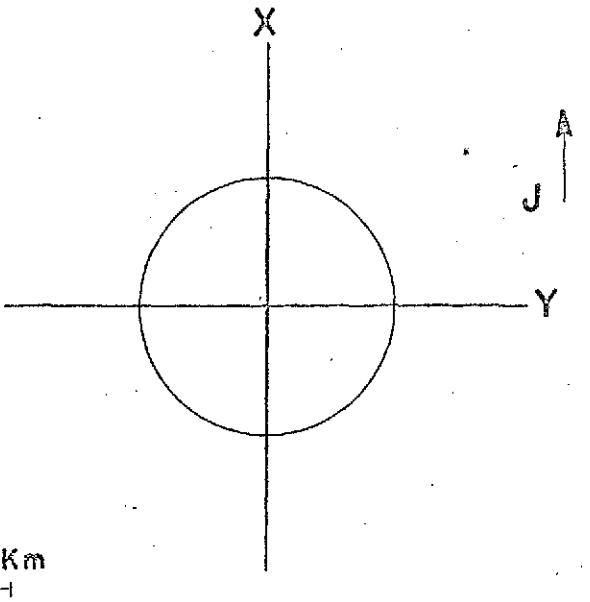

CRATER

MAGNETIZATION

INTENSITY = 10^{-5} emu
DECLINATION = 0.0 deg
INCLINATION = 0.0 deg

SATELLITE POSITION

x	y
0.0	0.0
20.00	0.0
40.00	0.0
60.00	0.0
80.00	0.0
100.00	0.0
120.00	0.0
140.00	0.0
160.00	0.0
180.00	0.0
200.00	0.0
220.00	0.0
240.00	0.0
260.00	0.0
280.00	0.0
300.00	0.0
320.00	0.0
340.00	0.0
360.00	0.0
380.00	0.0
400.00	0.0

ANOMALY

ΔX	ΔY	ΔZ
-0.721	0.000	0.000
-0.696	0.000	-0.209
-0.620	-0.000	-0.403
-0.496	0.000	-0.564
-0.335	0.000	-0.669
-0.163	0.000	-0.704
-0.011	0.000	-0.670
0.099	0.000	-0.590
0.163	-0.000	-0.493
0.191	0.000	-0.399
0.195	-0.000	-0.319
0.187	-0.000	-0.253
0.172	-0.000	-0.202
0.156	0.000	-0.161
0.140	0.000	-0.130
0.124	0.000	-0.106
0.111	0.000	-0.086
0.098	0.000	-0.071
0.087	0.000	-0.059
0.078	0.000	-0.049
0.069	-0.000	-0.041

SATELLITE HT. = 110 Km
RADIUS = 100 Km
DEPTH = 100 Km

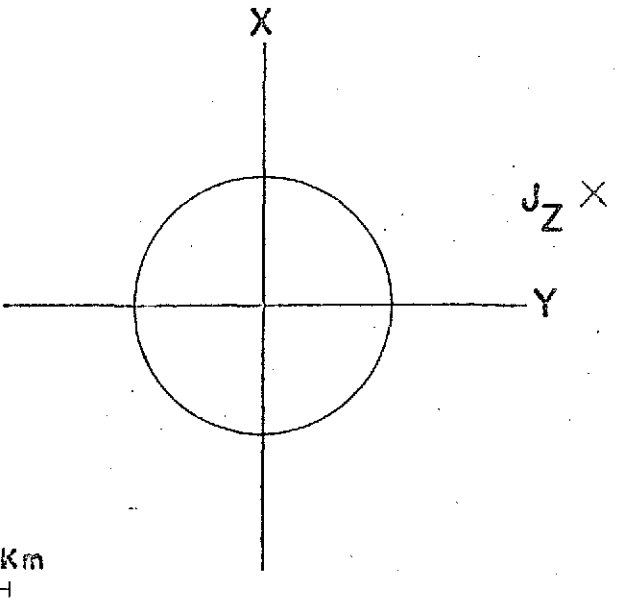

CRATER

MAGNETIZATION

INTENSITY = 10^{-5} emu
DECLINATION = 0.0 deg
INCLINATION = 90.0 deg

SATELLITE POSITION

x	y
0.0	0.0
20.00	0.0
40.00	0.0
60.00	0.0
80.00	0.0
100.00	0.0
120.00	0.0
140.00	0.0
160.00	0.0
180.00	0.0
200.00	0.0
220.00	0.0
240.00	0.0
260.00	0.0
280.00	0.0
300.00	0.0
320.00	0.0
340.00	0.0
360.00	0.0
380.00	0.0
400.00	0.0

ANOMALY

ΔX	ΔY	ΔZ
0.000	0.000	1.442
-0.209	0.000	1.408
-0.403	0.000	1.307
-0.564	0.000	1.141
-0.669	0.000	0.924
-0.704	0.000	0.684
-0.670	0.000	0.459
-0.590	0.000	0.278
-0.493	0.000	0.150
-0.399	0.000	0.068
-0.319	-0.000	0.018
-0.253	-0.000	-0.010
-0.202	0.000	-0.026
-0.161	0.000	-0.033
-0.130	0.000	-0.036
-0.106	0.000	-0.037
-0.086	0.000	-0.036
-0.071	-0.000	-0.034
-0.059	0.000	-0.032
-0.049	-0.000	-0.029
-0.041	0.000	-0.027

SATELLITE HT. = 110 Km
RADIUS = 200 Km
DEPTH = 20 Km

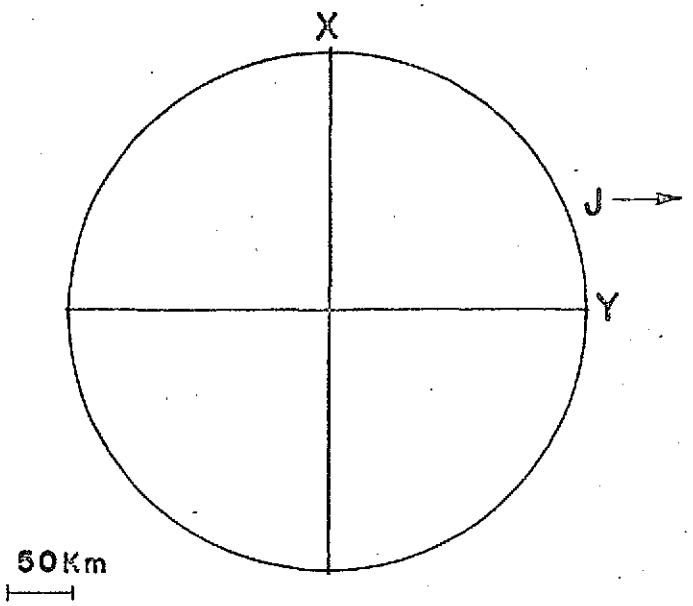

CRATER

MAGNETIZATION

INTENSITY = 10^{-5} emu
DECLINATION = 90.0 deg
INCLINATION = 0.0 deg

SATELLITE POSITION

x	y
0.0	0.0
20.00	0.0
40.00	0.0
60.00	0.0
80.00	0.0
100.00	0.0
120.00	0.0
140.00	0.0
160.00	0.0
180.00	0.0
200.00	0.0
220.00	0.0
240.00	0.0
260.00	0.0
280.00	0.0
300.00	0.0
320.00	0.0
340.00	0.0
360.00	0.0
380.00	0.0
400.00	0.0

ANOMALY

ΔX	ΔY	ΔZ
-0.000	-0.200	-0.000
-0.000	-0.200	0.000
-0.000	-0.200	0.000
0.000	-0.199	-0.000
-0.000	-0.197	0.000
-0.000	-0.194	0.000
-0.000	-0.189	0.000
0.000	-0.183	0.000
0.000	-0.174	0.000
0.000	-0.162	0.000
0.000	-0.148	0.000
0.000	-0.132	-0.000
-0.000	-0.116	-0.000
0.000	-0.101	-0.000
0.000	-0.087	0.000
-0.000	-0.074	0.000
0.000	-0.064	-0.000
0.000	-0.055	0.000
0.000	-0.047	0.000
0.000	-0.041	0.000
0.000	-0.035	0.000

SATELLITE HT. = 110 Km
RADIUS = 200 Km
DEPTH = 20 Km

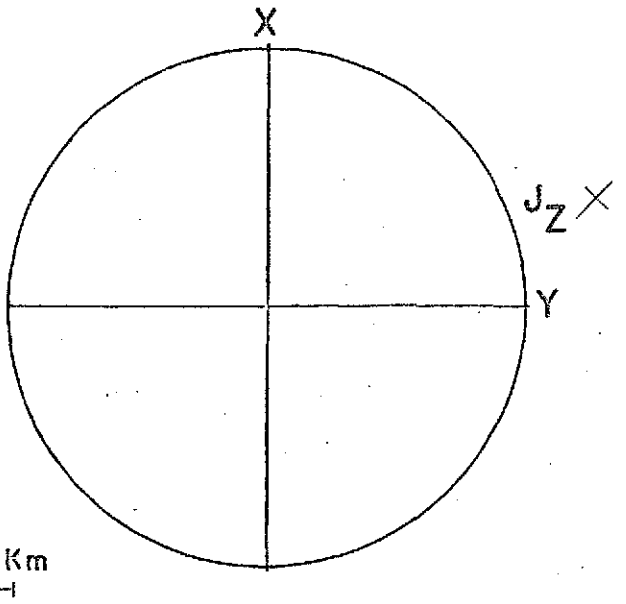

CRATER

MAGNETIZATION

INTENSITY = 10^{-5} emu
DECLINATION = 0.0 deg
INCLINATION = 90.0 deg

SATELLITE POSITION

x	y
0.0	0.0
20.00	0.0
40.00	0.0
60.00	0.0
80.00	0.0
100.00	0.0
120.00	0.0
140.00	0.0
160.00	0.0
180.00	0.0
200.00	0.0
220.00	0.0
240.00	0.0
260.00	0.0
280.00	0.0
300.00	0.0
320.00	0.0
340.00	0.0
360.00	0.0
380.00	0.0
400.00	0.0

ANOMALY

ΔX	ΔY	ΔZ
-0.000	-0.000	0.401
-0.027	0.000	0.400
-0.055	0.000	0.398
-0.084	0.000	0.393
-0.116	0.000	0.384
-0.150	0.000	0.369
-0.185	0.000	0.346
-0.218	0.000	0.312
-0.246	0.000	0.265
-0.261	0.000	0.208
-0.260	0.000	0.145
-0.242	0.000	0.087
-0.213	0.000	0.041
-0.178	0.000	0.008
-0.146	0.000	-0.013
-0.117	0.000	-0.024
-0.094	-0.000	-0.029
-0.075	0.000	-0.031
-0.060	0.000	-0.030
-0.049	0.000	-0.029
-0.039	0.000	-0.027

SATELLITE HT. = 110 Km
RADIUS = 200 Km
DEPTH = 40 Km

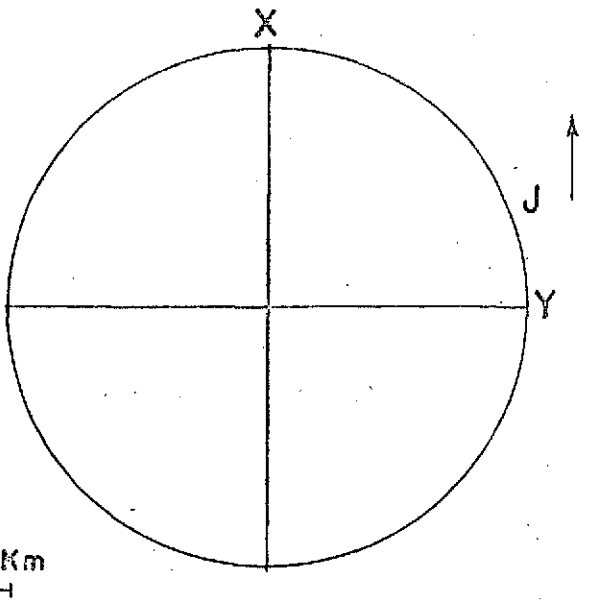

CRATER

MAGNETIZATION

INTENSITY = 10^{-5} emu
DECLINATION = 0.0 deg
INCLINATION = 0.0 deg

SATELLITE POSITION

x	y
0.0	0.0
20.00	0.0
40.00	0.0
60.00	0.0
80.00	0.0
100.00	0.0
120.00	0.0
140.00	0.0
160.00	0.0
180.00	0.0
200.00	0.0
220.00	0.0
240.00	0.0
260.00	0.0
280.00	0.0
300.00	0.0
320.00	0.0
340.00	0.0
360.00	0.0
380.00	0.0
400.00	0.0

ANOMALY

ΔX	ΔY	ΔZ
-0.384	0.000	-0.000
-0.383	0.000	-0.052
-0.379	0.000	-0.106
-0.370	0.000	-0.163
-0.356	0.000	-0.223
-0.333	0.000	-0.286
-0.297	0.000	-0.351
-0.244	0.000	-0.413
-0.174	0.000	-0.463
-0.089	0.000	-0.491
0.000	0.000	-0.489
0.078	0.000	-0.457
0.135	-0.000	-0.403
0.168	-0.000	-0.341
0.182	0.000	-0.281
0.181	0.000	-0.228
0.173	0.000	-0.184
0.160	0.000	-0.149
0.146	0.000	-0.121
0.132	0.000	-0.098
0.119	0.000	-0.081

SATELLITE HT. = 110 Km
RADIUS = 200 Km
DEPTH = 40 Km

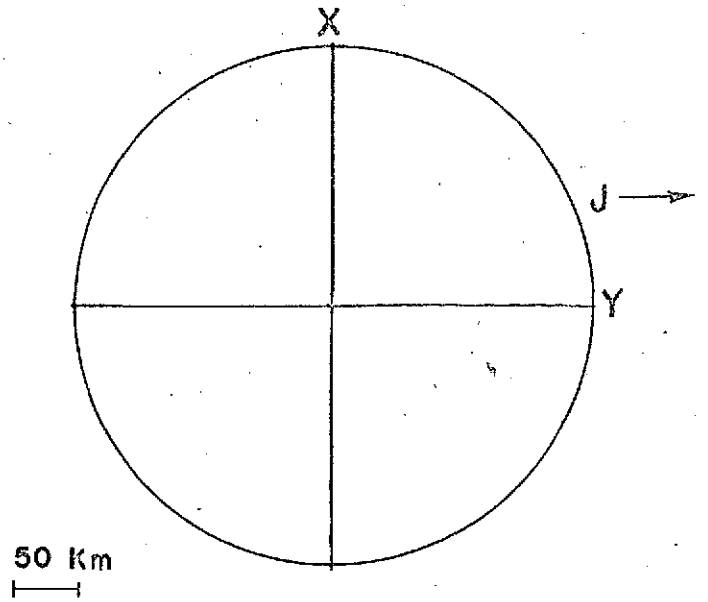

CRATER

MAGNETIZATION

INTENSITY = 10^{-5} emu
DECLINATION = 90.0 deg
INCLINATION = 0.0 deg

SATELLITE POSITION

x	y
0.0	0.0
20.00	0.0
40.00	0.0
60.00	0.0
80.00	0.0
100.00	0.0
120.00	0.0
140.00	0.0
160.00	0.0
180.00	0.0
200.00	0.0
220.00	0.0
240.00	0.0
260.00	0.0
280.00	0.0
300.00	0.0
320.00	0.0
340.00	0.0
360.00	0.0
380.00	0.0
400.00	0.0

ANOMALY

ΔX	ΔY	ΔZ
-0.000	-0.384	-0.000
-0.000	-0.384	0.000
-0.000	-0.382	0.000
-0.000	-0.380	-0.000
-0.000	-0.376	0.000
-0.000	-0.370	0.000
-0.000	-0.361	0.000
0.000	-0.348	0.000
-0.000	-0.331	0.000
0.000	-0.309	0.000
-0.000	-0.282	-0.000
0.000	-0.253	-0.000
-0.000	-0.223	-0.000
0.000	-0.194	0.000
-0.000	-0.167	0.000
-0.000	-0.144	0.000
-0.000	-0.124	-0.000
0.000	-0.107	0.000
-0.000	-0.092	-0.000
0.000	-0.080	0.000
-0.000	-0.070	-0.000

SATELLITE HT. = 110 Km
RADIUS = 200 Km
DEPTH = 40 Km

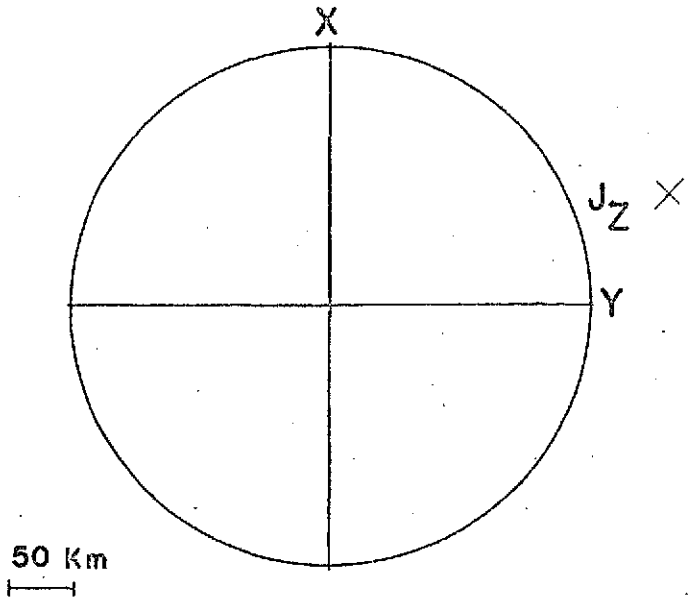

CRATER

MAGNETIZATION

INTENSITY = 10^{-5} emu
DECLINATION = 0.0 deg
INCLINATION = 90.0 deg

SATELLITE POSITION

x	y
0.0	0.0
20.00	0.0
40.00	0.0
60.00	0.0
80.00	0.0
100.00	0.0
120.00	0.0
140.00	0.0
160.00	0.0
180.00	0.0
200.00	0.0
220.00	0.0
240.00	0.0
260.00	0.0
280.00	0.0
300.00	0.0
320.00	0.0
340.00	0.0
360.00	0.0
380.00	0.0
400.00	0.0

ANOMALY

ΔX	ΔY	ΔZ
0.000	-0.000	0.768
-0.052	0.000	0.767
-0.106	0.000	0.761
-0.163	-0.000	0.750
-0.223	0.000	0.732
-0.286	0.000	0.702
-0.351	0.000	0.657
-0.413	0.000	0.592
-0.463	0.000	0.504
-0.491	0.000	0.397
-0.489	0.000	0.282
-0.457	0.000	0.174
-0.403	0.000	0.087
-0.341	0.000	0.025
-0.281	0.000	-0.014
-0.228	0.000	-0.037
-0.184	0.000	-0.049
-0.149	0.000	-0.053
-0.121	0.000	-0.054
-0.098	0.000	-0.052
-0.081	0.000	-0.049

SATELLITE HT. = 110 Km
RADIUS = 200 Km
DEPTH = 100 Km

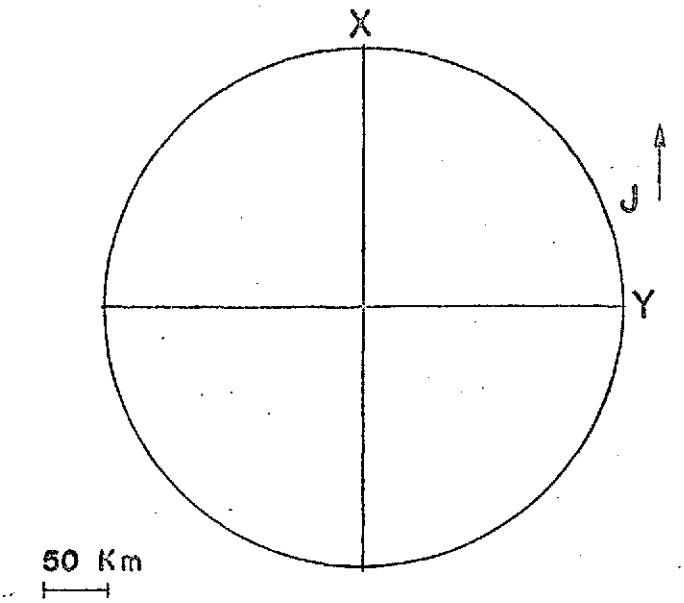

CRATER

MAGNETIZATION

INTENSITY = 10^{-5} emu
DECLINATION = 0.0 deg
INCLINATION = 0.0 deg

SATELLITE POSITION

x	y
0.0	0.0
20.00	0.0
40.00	0.0
60.00	0.0
80.00	0.0
100.00	0.0
120.00	0.0
140.00	0.0
160.00	0.0
180.00	0.0
200.00	0.0
220.00	0.0
240.00	0.0
260.00	0.0
280.00	0.0
300.00	0.0
320.00	0.0
340.00	0.0
360.00	0.0
380.00	0.0
400.00	0.0

ANOMALY

ΔX	ΔY	ΔZ
-0.906	-0.000	-0.000
-0.903	0.000	-0.122
-0.893	-0.000	-0.248
-0.874	0.000	-0.379
-0.841	0.000	-0.519
-0.788	0.000	-0.666
-0.706	0.000	-0.818
-0.586	0.000	-0.965
-0.422	0.000	-1.086
-0.222	0.000	-1.156
-0.012	0.000	-1.153
0.174	0.000	-1.077
0.307	-0.000	-0.951
0.384	-0.000	-0.807
0.414	0.000	-0.668
0.413	-0.000	-0.547
0.395	0.000	-0.446
0.368	-0.000	-0.365
0.337	0.000	-0.300
0.307	0.000	-0.247
0.278	0.000	-0.206

SATELLITE HT. = 110 Km
RADIUS = 200 Km
DEPTH = 100 Km

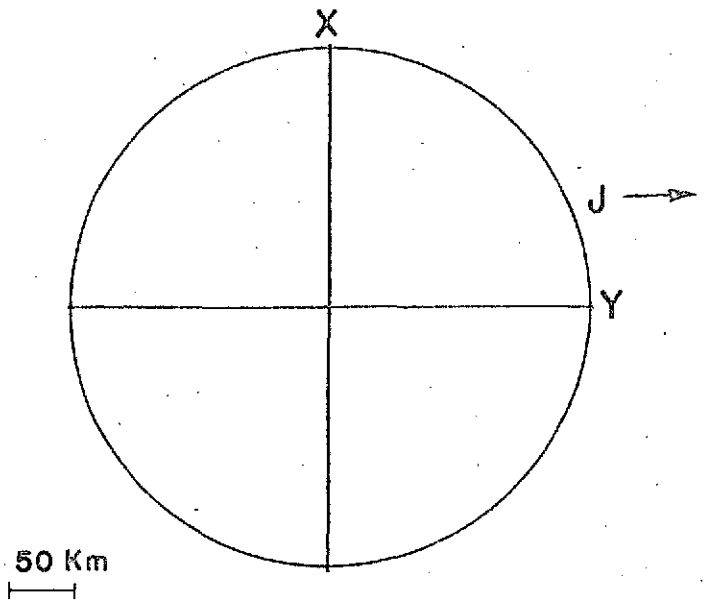

CRATER

MAGNETIZATION

INTENSITY = 10^{-5} emu
DECLINATION = 90.0 deg
INCLINATION = 0.0 deg

SATELLITE POSITION

x	y
0.0	0.0
20.00	0.0
40.00	0.0
60.00	0.0
80.00	0.0
100.00	0.0
120.00	0.0
140.00	0.0
160.00	0.0
180.00	0.0
200.00	0.0
220.00	0.0
240.00	0.0
260.00	0.0
280.00	0.0
300.00	0.0
320.00	0.0
340.00	0.0
360.00	0.0
380.00	0.0
400.00	0.0

ANOMALY

ΔX	ΔY	ΔZ
-0.000	-0.906	-0.000
-0.000	-0.905	0.000
-0.000	-0.902	-0.000
0.000	-0.896	-0.000
0.000	-0.887	0.000
-0.000	-0.873	0.000
-0.000	-0.852	0.000
0.000	-0.823	0.000
0.000	-0.784	0.000
0.000	-0.733	0.000
0.000	-0.671	-0.000
0.000	-0.602	-0.000
-0.000	-0.532	-0.000
0.000	-0.464	0.000
0.000	-0.402	0.000
-0.000	-0.347	0.000
0.000	-0.300	-0.000
-0.000	-0.260	0.000
0.000	-0.226	0.000
0.000	-0.197	0.000
0.000	-0.173	0.000

SATELLITE HT. = 110 Km
RADIUS = 200 Km
DEPTH = 100 Km

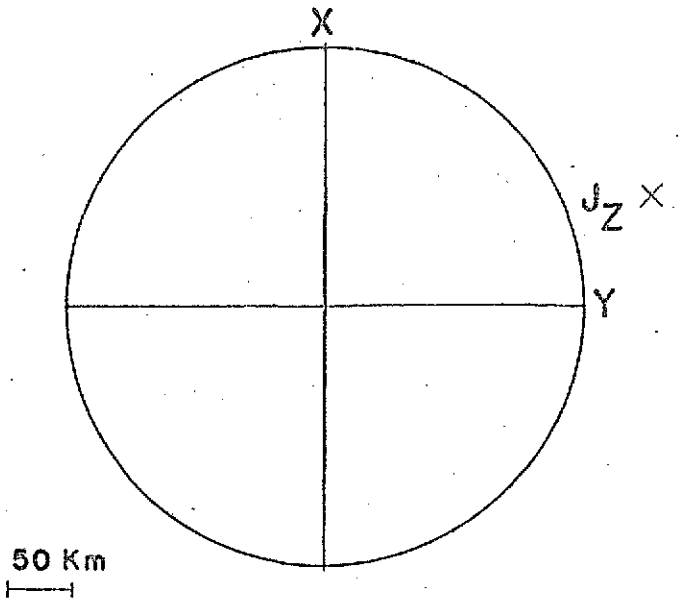

CRATER

MAGNETIZATION

INTENSITY = 10^{-5} emu
DECLINATION = 0.0 deg
INCLINATION = 90.0 deg

SATELLITE POSITION

x	y
0.0	0.0
20.00	0.0
40.00	0.0
60.00	0.0
80.00	0.0
100.00	0.0
120.00	0.0
140.00	0.0
160.00	0.0
180.00	0.0
200.00	0.0
220.00	0.0
240.00	0.0
260.00	0.0
280.00	0.0
300.00	0.0
320.00	0.0
340.00	0.0
360.00	0.0
380.00	0.0
400.00	0.0

ANOMALY

ΔX	ΔY	ΔZ
-0.000	-0.000	1.812
-0.122	0.000	1.808
-0.248	0.000	1.795
-0.379	-0.000	1.770
-0.519	0.000	1.727
-0.666	0.000	1.660
-0.818	0.000	1.558
-0.965	0.000	1.409
-1.086	0.000	1.206
-1.156	0.000	0.955
-1.153	0.000	0.683
-1.077	0.000	0.429
-0.951	0.000	0.225
-0.807	0.000	0.080
-0.668	0.000	-0.012
-0.547	0.000	-0.066
-0.446	0.000	-0.095
-0.365	0.000	-0.108
-0.300	0.000	-0.111
-0.247	0.000	-0.110
-0.206	0.000	-0.105